RESEARCH ARTICLE

Rice LIKE EARLY STARVATION1 cooperates with FLOURY ENDOSPERM 6 to modulate starch biosynthesis and endosperm development

Haigang Yan,[a,1] Wenwei Zhang,[a,c,1] Yihua Wang,[a,c,1] Jie Jin,[a] Hancong Xu,[a] Yushuang Fu,[a] Zhuangzhuang Shan,[a] Xin Wang,[b] Xuan Teng,[a] Xin Li,[a] Yongxiang Wang,[a] Xiaoqing Hu,[a] Wenxiang Zhang,[a] Changyuan Zhu,[a] Xiao Zhang,[a] Yu Zhang,[a] Rongqi Wang,[a] Jie Zhang,[a] Yue Cai,[a] Xiaoman You,[a] Jie Chen,[a] Xinyuan Ge,[a] Liang Wang,[a] Jiahuan Xu,[a] Ling Jiang,[a,c] Shijia Liu,[a,c] Cailin Lei,[b] Xin Zhang,[b] Haiyang Wang,[b] Yulong Ren,[b,2] and Jianmin Wan[a,b,c,2]

[a]State Key Laboratory of Crop Genetics & Germplasm Enhancement and Utilization, Nanjing Agricultural University, Nanjing 210095, China

[b]State Key Laboratory of Crop Gene Resources and Breeding, Institute of Crop Sciences, Chinese Academy of Agricultural Sciences, Beijing 100081, China

[c]Zhongshan Biological Breeding Laboratory, Nanjing 210095, China

[1]These authors contributed equally (H.Y., W.Z., and Y.W.)

Short title: Regulation of amylopectin biosynthesis in rice

[2]Corresponding authors: Jianmin Wan (wanjm@njau.edu.cn), Yulong Ren (renyulong@caas.cn)

The authors responsible for distribution of materials integral to the findings presented in this

article in accordance with the policy described in the Instructions for Authors (https://academic.oup.com/plcell) are: Jianmin Wan (wanjm@njau.edu.cn) and Yulong Ren (renyulong@caas.cn).

Keywords: Rice (*Oryza sativa*), LESV, FLO9, FLO6, ISA1, starch biosynthesis, endosperm development

Abstract

In cereal grains, starch is synthesized by the concerted actions of multiple enzymes on the surface of starch granules within the amyloplast. However, little is known about how starch-synthesizing enzymes access starch granules, especially for amylopectin biosynthesis. Here, we show that the rice (*Oryza sativa*) *floury endosperm9* (*flo9*) mutant is defective in amylopectin biosynthesis, leading to grains exhibiting a floury endosperm with a hollow core. Molecular cloning revealed that *FLO9* encodes a plant-specific protein homologous to Arabidopsis (*Arabidopsis thaliana*) LIKE EARLY STARVATION1 (LESV). Unlike Arabidopsis LESV, which is involved in starch metabolism in leaves, OsLESV is required for starch granule initiation in the endosperm. OsLESV can directly bind to starch by its C-terminal tryptophan (Trp)-rich region. Cellular and biochemical evidence suggests that OsLESV interacts with the starch-binding protein FLO6, and loss-of-function mutations of either gene impair ISOAMYLASE 1 (ISA1) targeting to starch granules. Genetically, *OsLESV* acts synergistically with *FLO6* to regulate starch biosynthesis and endosperm development. Together, our results identify OsLESV–FLO6 as a non-enzymatic molecular module responsible for ISA1 localization on starch granules, and present a target gene for use in biotechnology to control starch content and composition in rice endosperm.

IN A NUTSHELL

Background: Starch accounts for up to 75% of grain weight, and greatly affects cereal crop yield and quality. Significant advances have been made in the functional characterization of starch

metabolism enzymes in cereal crops. In addition to starch metabolism enzymes, some non-enzymatic players with starch-binding domains play crucial roles in starch biosynthesis. ISOAMYLASE1 (ISA1), a type of debranching enzyme unable to bind starch, functions in starch biosynthesis through removing superfluous branch points. However, how ISA1 is targeted to starch granules remains largely unknown.

Question: Comparable phenotypic defects between *floury endosperm 9* (*flo9*) and *isa1* prompted us to propose that LIKE EARLY STARVATION1 (OsLESV), the target protein responsible for the *flo9* phenotype, might regulate rice (*Oryza sativa*) starch biosynthesis by associating with ISA1. Therefore, we asked whether OsLESV is a non-enzymatic player that facilitates ISA1 targeting to starch.

Findings: We determined that the rice *flo9* mutant is defective in starch biosynthesis and endosperm development, similar to the reported *isa1* mutants. *FLO9* encodes an amyloplast-localized protein homologous to Arabidopsis (*Arabidopsis thaliana*) LESV. OsLESV is required for compound starch granule initiation in the endosperm. OsLESV directly binds to starch by its C-terminal Trp-rich region. We demonstrated that OsLESV interacts with the reported non-enzymatic player FLO6, and loss-of-function of either gene impairs ISA1 targeting to starch granules. Genetically, *OsLESV* acts synergistically with *FLO6* to modulate starch biosynthesis and endosperm development. Our findings establish a molecular link between non-enzymatic players and ISA1 in rice starch biosynthesis and endosperm development.

Next steps: In addition to facilitating ISA1 localization on starch granules, OsLESV likely exerts other functions in starch biosynthesis and endosperm development. Therefore, it is important to identify other unknown cargos to fully understand the biological significance of OsLESV in regulating starch metabolism in future studies.

Introduction

Starch accounts for up to 75% of grain weight and therefore greatly affects cereal crop yield and quality. Starch is composed of two types of glucose polymers, amylose and amylopectin, with the latter constituting 75–80% of starch weight (Le Corre et al., 2010; Bao, 2019). Amylose is a linear polymer comprising D-glucose molecules connected via α-1,4-linkages, whereas amylopectin is a highly branched, huge polymer formed by regular α-1,6-glycosidic linkages of linear polymers (Jenkins et al., 1993; Thompson, 2000).

Starch biosynthesis in the endosperm of cereals occurs in amyloplasts, in which amylose and amylopectin together form insoluble, semicrystalline particles termed starch grains (SGs). SGs are either compound or single, depending on the species (Matsushima et al., 2010; Myers et al., 2011; Seung et al., 2018; Abt and Zeeman,

2020). Amylopectin branches that are arranged in clusters can form stable double helices whose packing leads to the formation of crystalline layers of starch granules, whereas amylose appears to be interspersed among amylopectin clusters within starch granules (Zeeman et al., 2010; Abt and Zeeman, 2020; Smith and Zeeman, 2020). Although starch in cereal endosperm provides a major calorie source for human food and animal feed, our understanding of the molecular machinery that controls starch biosynthesis in cereal crops remains obscure.

The biosynthesis of amylopectin in starch granules requires the orchestrated activities of at least three distinct classes of enzymes (Ball et al., 1996; Nakamura, 2002; James et al., 2003; Fujita et al., 2006; Hanashiro et al., 2008; Abt and Zeeman, 2020). Starch synthases (SSs) elongate linear glucan chains using ADP-glucose as the glucose donor. Starch branching enzymes (BEs) are responsible for introducing α-1,6 branch points, whereas the two types of starch debranching enzymes (DBEs), isoamylase (ISA) and pullulanase (PUL), are required to remove superfluous or improper branch points to produce crystallization-competent glucans (Kubo et al., 1999). By contrast, the biosynthesis of amylose within the amylopectin matrix only involves granule-bound starch synthase (GBSS). Upon entering the amyloplast or chloroplast, several starch-synthesizing enzymes such as rice (*Oryza sativa*) starch branching enzyme I (OsBEI), Arabidopsis (*Arabidopsis thaliana*) starch synthesis III (AtSSIII), and Arabidopsis branching enzyme I (AtBEI) directly associate with starch granules via their own starch-binding domains (Dumez et al., 2006; Valdez et al., 2008; Chaen et al., 2012). Amylopectin-synthesizing enzymes, especially SSs and BEs, form large enzymatically active protein complexes in the amyloplast stroma, thereby facilitating their attachment to starch granules (Liu et al., 2012; Crofts et al., 2015). Notably, ISAs are absent from these complexes (Crofts et al., 2015), and *in vitro* studies showed that ISA1 essential for amylopectin biosynthesis in rice endosperm cannot bind to starch directly (Peng et al., 2014). Therefore, the molecular mechanism by which ISA1 targets to starch granules remains unclear.

In addition to the starch metabolic enzymes themselves, accumulating evidence suggests that some non-enzymatic players with starch-binding domains, such as

carbohydrate binding module 48 (CBM48), play crucial roles in starch metabolism (Abt and Zeeman, 2020; Smith and Zeeman, 2020). Rice CBM48 domain-containing FLOURY ENDOSPERM6 (FLO6) is genetically characterized as a non-enzymatic player, which is proposed to function as a starch-binding protein in starch biosynthesis and compound granule formation through a direct interaction with ISA1 (Peng et al., 2014). By contrast, the Arabidopsis FLO6 homolog, PROTEIN TARGETING TO STARCH2 (PTST2) is involved in starch granule initiation in leaves through supplying STARCH SYNTHASE4 (SS4) with pre-selected malto-oligosaccharides (Seung et al., 2017). Arabidopsis PTST1, which is structurally similar to FLO6, interacts with and targets GBSS to the amorphous regions of starch granules; its loss of function substantially influences amylose production in leaves (Seung et al., 2015). Unexpectedly, PTST1 depletion in rice has negligible effects on amylose content in endosperm (Wang et al., 2020). The functional differences in these non-enzymatic proteins suggest that different species and even tissues likely employ distinct sets of non-enzymatic players in orchestrating highly complex starch synthesis. Despite these significant advances, our understanding of the biological roles of these non-enzymatic proteins in starch synthesis remains very limited, especially in cereal crops.

In this study, as part of our continuous effort to understand the molecular machinery responsible for starch biosynthesis in rice endosperm, we isolated and functionally characterized the rice *floury endosperm9* (*flo9*) mutant. The *flo9* mutant is defective in amylopectin biosynthesis and partially phenocopies the rice *isa1* mutants, which accumulate an assortment of water-soluble-glucans (WSGs) instead of starch in the endosperm (Nakamura et al., 1997; Fujita et al., 2003; Nakagami et al., 2017). *FLO9* encodes an amyloplast-localized protein homologous to Arabidopsis LIKE EARLY STARVATION1 (LESV), which is involved in starch metabolism in Arabidopsis leaves (Feike et al., 2016). We presented biochemical and confocal microscopy evidence supporting the notion that OsLESV physically interacts with ISA1 and that its loss of function significantly perturbs the targeting of ISA1 to starch granules. Furthermore, we establish a mechanistic linkage between OsLESV and FLO6, and propose that they form a functional protein complex to cooperatively

modulate starch biosynthesis and endosperm development. Taken together, our findings identify OsLESV as a non-enzymatic regulator that positively modulates amylopectin synthesis in rice endosperm.

Results

The *flo9* mutant exhibits a defect in amylopectin accumulation in endosperm

To better understand the molecular mechanisms underlying starch biosynthesis in rice, we conducted a forward genetic screen to identify mutants defective in starch accumulation from an *N*-methyl-*N*-nitrosourea-mutagenized mutant library of the elite *japonica* rice variety W017. One such mutant, *flo9*, produced floury and shrunken endosperm with dimpled indentations and constrictions at the dorsal and ventral sides, respectively, in sharp contrast to the translucent, plump endosperm of the wild type (Figure 1A). Microscopy analysis of transverse sections showed that *flo9* endosperm is composed of a translucent periphery, a floury-white intermediate region filled with aberrantly loose SGs, and a hollow core (Figure 1, B and C). These endosperm defects in *flo9* led to a 16.8% loss in 1000-grain weight compared to the wild type (Supplemental Figure S1A).

Iodine staining revealed two different areas of endosperm in *flo9*: a well-stained area corresponding to the translucent and floury regions, and a barely stained area corresponding to the hollow core (Figure 1D). Quantification showed that, compared to the wild type, total starch and amylopectin contents were reduced, whereas amylose, protein, and lipid contents were increased (Supplemental Figure S1, B–G). To further investigate the causal effect of the *flo9* mutation on storage substance accumulation, we presented the contents of storage substances per grain given the decreased grain weight. Strikingly, amylose and protein contents were unaffected, whereas total starch and amylopectin contents were reduced by 31.7% and 38.05%, respectively (Figure 1E; Supplemental Figure S1H). These results indicate a possible specific defect in amylopectin biosynthesis in *flo9*. The increase of lipid content may be due to a secondary effect of disrupted starch biosynthesis, as reported previously for many

floury endosperm mutants such as *flo10*, *flo15*, and *floury shrunken endosperm5* (*fse5*) (Wu et al., 2019; You et al., 2019; Wang et al., 2021).

Given the spatial phenotypic difference of *flo9* endosperm (Figure 1B), we separately examined the chain-length distribution (CLD) of total glucans in peripheral, intermediate, and central regions of *flo9* endosperm. As shown in Figure 1F, the glucan CLD in *flo9* peripheral region varied little from that of wild type, while the glucan CLD in *flo9* intermediate region exhibited a moderate increase in short chains spanning 6 to 11 degrees of polymerization (DP) and a subtle decrease in intermediate chains compared with those of wild type. Strikingly, we observed a dramatic increase in short chains of $6 < DP < 14$ and a relatively gentle variation in intermediate chains in the central part of *flo9* endosperm (Figure 1F).

The absent iodine staining and abnormal glucan CLD in *flo9* central regions were most reminiscent of the *isa1* mutants, which accumulate WSGs instead of amylopectin (Nakamura et al., 1997; Nakagami et al., 2017). Supporting this notion, the WSG content was considerably elevated in *flo9* relative to the wild type (Figure 1E). Consistent with disrupted starch biosynthesis, both the starch pasting properties and gelatinization properties were also affected in *flo9* (Supplemental Table S1; Supplemental Figure S1, I–K). Together, these results indicate that the *flo9* mutation predominantly affects amylopectin biosynthesis in rice endosperm.

The *flo9* mutation disturbs compound starch granule initiation

To investigate the cellular basis of the abnormal starch accumulation observed in *flo9*, we prepared semi-thin and thick sections of developing grains at 6, 9 and 12 days after flowering (DAF). In line with Figure 1D, SGs in the peripheral and intermediate parts of *flo9* endosperm were well-stained with iodine, whereas SGs in the central part of *flo9* endosperm, if any, were barely stained (Supplemental Figure S2, A and B). To further investigate the origin and formation of the hollow core observed in *flo9*, we stained thick sections of wild-type and *flo9* developing endosperm using a non-specific β-glucan dye, Calcofluor White. As shown in Supplemental Figure S2C, similar to wild type, the cell wall structures were readily observed in *flo9* central

endosperm cells early at 6 DAF. These results suggest that the central cells of *flo9* endosperm are formed normally but devoid of typical SGs.

We next compared the morphological differences of SGs in peripheral, intermediate, and central endosperm cells between the wild type and *flo9*. The sizes of amyloplasts gradually increased from the outside to inside of endosperm in the wild type, and all the amyloplasts contained polyhedral, sharp-edged, and well-defined granules (Figure 2, A–C and G–I). At the endosperm periphery, the size and morphology of amyloplasts were largely comparable between the wild type and *flo9* (Figure 2, A, D, G, and J). Compared with the characteristic sharp-edged granules in the intermediate part of wild-type endosperm at 9 DAF (Figure 2B), amyloplasts in *flo9* were filled with numerous scattered, tiny granules at the same stage (Figure 2E).

During endosperm development, a large, amorphous structure with a dark-stained edge formed inside amyloplasts in the *flo9* intermediate regions (Figure 2K). Notably, we readily observed atypical amyloplasts lacking compound granules in the central part of *flo9* early at 9 DAF (Figure 2F). These abnormal amyloplasts in *flo9* were also observed in our previously reported *flo6* mutant, suggesting that both proteins most likely play a similar functional role in modulating amyloplast development (Peng et al., 2014). Consistent with the increased levels of WSGs in the *flo9* mutant (Figure 1E), the central part of *flo9* endosperm was mainly filled with pink-stained substances (Figure 2, F and L; Supplemental Figure S2D), likely corresponding to phytoglycogen, as reported previously for *isa1* (Nakamura et al., 1997; Matsushima et al., 2010; Nagamatsu et al., 2022). Taken together, these results suggest that the loss of *FLO9* function affects compound starch granule initiation in rice endosperm, especially in the intermediate and central parts.

***FLO9* encodes an Arabidopsis LESV homolog OsLESV that is predominantly expressed in endosperm**

For genetic analysis, we performed a reciprocal cross between *flo9* and the wild type. In the F_2 progeny, wild-type grains and *flo9* grains segregated with a ratio of

242 approximately 3:1 (Supplemental Table S2), indicating that the *flo9* phenotype is
243 controlled by a single recessive nuclear gene. To isolate the causal gene, we generated
244 an F_2 segregating population by crossing *flo9* with the *indica* variety Nanjing 11.
245 Using 969 individuals with the *flo9* phenotype from the F_2 population, we delimited
246 the target locus to a 253-kb genomic region on chromosome 11 containing 31 putative
247 open reading frames (Figure 3A). Genomic sequencing revealed a C-to-A substitution
248 within the first exon of Os11g0586300 (*OsLESV*; Feike et al., 2016), which putatively
249 introduces a premature stop codon in place of the wild-type Ser-64 residue (Figure
250 3B).

251 To test whether the mutation in *OsLESV* is responsible for the *flo9* phenotypes, we
252 introduced a construct harboring the full-length coding sequence of *OsLESV* driven
253 by its native 1,972-bp promoter into homozygous *flo9* calli for complementation test.
254 Seeds collected from three T_4 generation transgenic lines showed a complete
255 restoration of the wild-type phenotypes, including grain appearance, compound
256 granule arrangement as well as both starch and amylopectin contents (Figure 3, C–E).
257 We also generated three independent knockout mutants of *OsLESV* using the
258 CRISPR/Cas9-mediated genome editing technology (Supplemental Figure S3A).
259 Grains harvested from these mutant lines phenocopied the *flo9* mutant (Supplemental
260 Figure S3, B and C). Furthermore, we raised polyclonal antibodies against OsLESV,
261 which specifically recognized a protein with the expected size in immunoblots of
262 mature grain extracts from the wild type and complemented transgenic lines, but not
263 from the *flo9* or knockout mutants (Figure 3F; Supplemental Figure S3D), confirming
264 the effectiveness and specificity of the anti-OsLESV antibodies. Together, these
265 results demonstrate that OsLESV is indeed the causal gene responsible for the *flo9*
266 phenotypes.

267 *OsLESV* is predicted to encode a protein of unknown function composed of 618
268 amino acids that harbors a tryptophan (Trp)-rich region at its C terminus
269 (Supplemental Figure S4A). The point mutation in *OsLESV* of the *flo9* mutant
270 introduces a premature stop codon; if the truncated protein accumulates, it would
271 completely lack the conserved Trp-rich region. A BLAST search showed that

OsLESV is a single copy gene in the rice genome, but it is highly conserved among starch-synthesizing organisms including land plants and green algae (Supplemental Figure S4, B and C). Arabidopsis LESV is reported to be involved in starch metabolism in Arabidopsis leaves (Feike et al., 2016). Similarly, the loss of *OsLESV* function also significantly affected starch turnover in leaves over the day-night cycle, as demonstrated by the disrupted starch and soluble sugar metabolisms (Supplemental Figure S5).

To investigate the protein accumulation pattern of OsLESV in wild-type plants, we performed an immunoblot analysis of total protein extracts from multiple tissues: roots, stems, leaves, leaf sheaths, panicles, and endosperm at different stages of development. As shown in Figure 3G, we detected OsLESV protein in all tissues tested, with substantially higher levels in developing endosperm, where it increased during grain filling and peaked at 12 DAF, then subsided.

Because *flo9* exhibited the most severe developmental defects in inner endosperm cells, we expected that OsLESV might be abundant in the interior of the grain. To test this notion, we divided developing endosperm into the outer and inner parts, and mature brown grains into the periphery, intermediate, and center, followed by a quantitative immunoblot analysis. OsLESV abundance did show a gradient increase from the exterior to the interior in both developing and mature endosperm (Figure 3, H and I), which was consistent with the endosperm defects of *flo9* (Figure 1B). Together, these results demonstrate that OsLESV is a plant-specific protein with higher abundance in endosperm, especially in the interior region.

OsLESV associates with SGs by directly binding to starch

The online tool TargetP predicted that OsLESV harbors a 38-amino acid chloroplast transit peptide (cTP) at its N terminus (Emanuelsson et al., 1999; Supplemental Figure S4A). To confirm the plastid localization of OsLESV, we transiently transfected a *Pro35S:OsLESV-GFP* (*green fluorescent protein*) construct into rice protoplasts. The OsLESV-GFP fusion protein exhibited a disc-like localization pattern within chloroplasts (Figure 4A). To ascertain whether these structures represent SGs, we

co-transfected *Pro35S:OsLESV-GFP* with *Pro35S:GBSSII-mCherry*, encoding a SG-bound marker protein fused to the fluorescent protein mCherry (Dian et al., 2003), into rice protoplasts. Notably, both fusion proteins co-localized within chloroplasts (Figure 4B).

To clarify the domain responsible for OsLESV localization, we generated several fusions between GFP and OsLESV domain truncations. As expected, deletion of the cTP motif (OsLESVΔcTP$^{1\text{-}38}$-GFP) abolished the chloroplast localization of OsLESV (Figure 4C). By contrast, the N-terminal 345 amino acid fragment of OsLESV (OsLESVΔCT$^{346\text{-}618}$-GFP) localized to chloroplasts but exhibited a diffuse signal at the chloroplast periphery, instead of the disc-like signal presented by the full-length protein (Figure 4D). These results indicate the important role of the C-terminal Trp-rich region for intra-chloroplast distribution of OsLESV-GFP. Moreover, a chimeric OsLESV protein with cTP fused with the C-terminal region (OsLESVΔNT$^{39\text{-}345}$-GFP) co-localized with GBSSII-mCherry (Figure 4E), and the mutation of 16 evolutionarily conserved Trp residues to alanine (Ala) (OsLESVΔNT$^{39\text{-}345}$[16W-16A]-GFP) abolished the localization of OsLESV to SGs (Figure 4F; Supplemental Figure S6A). These results indicate that OsLESV is associated with SGs and that its C-terminal Trp-rich region is essential for its sub-plastid localization.

To evaluate the intracellular localization of OsLESV in developing endosperm, we introduced an *OsLESV-GFP* construct into the *flo9* background under the control of the native *OsLESV* regulatory elements, namely its promoter, intron, and downstream regulatory region (Supplemental Figure S7A). The appearance of transgenic grains that accumulated the OsLESV-GFP fusion protein was fully restored to that of the wild type (Supplemental Figure S7, B–D), demonstrating that the OsLESV-GFP fusion protein is biologically functional. Moreover, we also introduced the *OsLESV-GFP* fusion construct driven by the *UBIQUITIN* promoter into the *flo9* mutant. Transgenic grains with high levels of OsLESV-GFP, as manifested by immunoblotting, also exhibited a wild-type translucent appearance (Supplemental Figure S8). Furthermore, we performed immuno-gold electron microscopy of

ultra-thin sections prepared from the *ProUbi:OsLESV-GFP* transgenic endosperm cells in the *flo9* background. As shown in Supplemental Figure S9, gold particles were detected particularly on the starch granules and amyloplast stroma.

To examine whether OsLESV indeed associates with SGs in developing endosperm, we performed a subcellular fractionation assay, followed by immuno-detection with protein-specific antibodies. Accordingly, we separated proteins from developing endosperm into three distinct fractions: soluble proteins (S), proteins loosely bound to SGs (LBP), and proteins tightly bound to SGs (TBP). LBP corresponds to proteins that are loosely adsorbed to the granule surface and easily separated by extensive washes or protease digestion, while TBPs are tightly encapsulated into granules and isolated only in boiling SDS buffer (Boren et al., 2004; Grimaud et al., 2008). Immunoblot analysis showed that OsLESV is present in all three protein fractions, with relatively higher proportions in the S and LBP than in the TBP fraction (Figure 4G). Notably, ISA1 accumulated only in the S and LBP fractions (Figure 4G). As controls, we detected FLO4 (a pyruvate orthophosphate dikinase B [PPDKB]) and GBSSI exclusively in S and TBP, respectively, whereas BEI was present in both the S and LBP fractions (Figure 4G), which is consistent with previous reports (Utsumi et al., 2011; Hayashi et al., 2018).

To determine whether OsLESV binds to starch directly, we conducted an *in vitro* glucan binding assay (Figure 4, Supplemental Figure S6B). As control, we used non-starch substance Sephadex G-10 beads to exclude the non-specific binding or protein precipitation (Abt et al., 2020; David et al., 2022), and the results showed that no proteins were detected after the final wash (Figure 4H). Notably, recombinant glutathione S-transferase (GST)-OsLESV protein, but not free GST protein, was able to bind to both amylopectin and amylose (Figure 4, I and J).

Truncation analysis showed that the C-terminal Trp-rich region of OsLESV is responsible for its binding to starch (Figure 4K). To investigate the role of conserved Trp residues in the ability of OsLESV binding to starch, we first evaluated the folding status of GST-OsLESV-CT and GST-OsLESV-CT(16W-16A) recombinant proteins using the circular dichroism (CD) spectroscopy. The results showed that both proteins

exhibited similar secondary structure, indicating that the 16 evolutionarily conserved Trp residues mutations did not obviously affect the folding of OsLESV (Supplemental Figure S6, C–E). Consistent with the effect of mutated Trp residues on the subcellular localization of OsLESV (Figure 4F), these mutations completely abolished OsLESV binding to starch (Figure 4L). Together, these results suggest that OsLESV associates with SGs by virtue of its C terminus, similar to Arabidopsis LESV (Liu et al., 2023).

OsLESV **is required for the targeting of ISA1 to SGs**

These findings that *flo9* partially phenocopied *isa1* mutants (Figures 1 and 2) and that OsLESV shared a similar expression pattern with ISA1 in developing endosperm (Supplemental Figure S10) prompted us to investigate whether OsLESV functions cooperatively with ISA1 in regulating endosperm starch biosynthesis. To this end, we performed yeast (*Saccharomyces cerevisiae*) two-hybrid (Y2H) assay to assess the possible interaction between OsLESV and ISA1. Strikingly, Y2H assay showed that OsLESV strongly interacts with ISA1 in yeast (Figure 5A; Supplemental Figure S11). Domain truncation analysis further showed that the N terminus (OsLESVΔCT$^{346\text{-}618}$), but not the C terminus (OsLESVΔNT$^{1\text{-}345}$) of OsLESV specifically binds to ISA1 (Figure 5A). We verified the interaction between OsLESV and ISA1 *in vitro* using a pull-down assay and *in vivo* using a firefly luciferase complementation imaging (LCI) assay in *Nicotiana benthamiana* leaf epidermal cells (Figure 5, B and C). Moreover, we confirmed the direct interaction of OsLESV and ISA1 by conducting an *in vivo* co-immunoprecipitation assay with lysates from transfected rice protoplasts (Figure 5D). Together, these results suggest that OsLESV specifically interacts with ISA1 via its N-terminal region.

We then investigated the effect of OsLESV depletion on subcellular localization of the ISA1-GFP fusion protein (with GFP fused to its C terminus) in rice protoplasts. As shown in Supplemental Figure S12, when co-expressed with *GBSSII-mCherry* in wild-type protoplasts, the ISA1-GFP fusion protein partially co-localized with GBSSII-mCherry onto SGs (Supplemental Figure S12A). Notably, when co-expressed with *GBSSII-mCherry* in *flo9* protoplasts, the colocalization of both

fusion proteins was largely compromised (Supplemental Figure S12B). This altered localization of ISA1-GFP in different background protoplasts was not due to the expression difference of ISA1-GFP, as assessed by quantitative immunoblot analyses (Supplemental Figure S12, C and D). These results suggested that OsLESV is required for the association of ISA1 with SGs.

Moreover, we validated the impaired targeting of ISA1 to SGs by a subcellular fractionation assay, followed by quantitative immunoblot analysis. Compared to the wild type, we observed a decreased amount of ISA1 in the loosely bound protein fraction (LBP) in *flo9* developing endosperm (Figure 5, E and F). Interestingly, immunoblotting combined with quantitative analysis also showed that ISA1 protein levels were significantly reduced in total protein extracts from *flo9* endosperm compared to the wild type (Figure 5, E and F). Together, these results suggest that OsLESV plays an important role in the delivery of ISA1 to starch granules, and its depletion compromised the abundance of endogenous ISA1 protein.

OsLESV physically interacts with FLO6 through their N termini

We previously demonstrated that FLO6 also interacts with ISA1 and starch (Peng et al., 2014). Subcellular fractionation assay further verified that FLO6 depletion influences the association of ISA1 with starch (Supplemental Figure S13, A–E). Based on the phenotypic defects in compound granule formation and biochemical evidence, we reasoned that OsLESV might associate with FLO6 to regulate starch biosynthesis, and thus performed Y2H assays to test this hypothesis. Indeed, OsLESV exhibited a strong interaction with FLO6 (Figure 6A; Supplemental Figure S13F). Domain truncation analysis revealed that the N termini of both OsLESV and FLO6 are required for their interaction (Figure 6A; Supplemental Figure S13F). We further verified the interaction using an *in vitro* pull-down assay as well as an *in vivo* LCI assay in *N. benthamiana* leaf epidermal cells (Figure 6, B and C). Together, these results suggest that OsLESV physically interacts with FLO6 *in vivo*.

Given that both OsLESV and FLO6 can interact with ISA1, we hypothesized that OsLESV might act together with FLO6 to facilitate the access of ISA1 to starch

granules. Quantitative analysis of β-galactosidase activity in a yeast three-hybrid assay and an *in vivo* LCI assay revealed that *FLO6* expression significantly enhances the strength of the interaction between OsLESV and ISA1, and vice versa (Figure 6, D and E; Supplemental Figure S14). Furthermore, we performed an *in vitro* starch binding assay to investigate whether OsLESV and FLO6 function together to facilitate the binding of ISA1 to amylopectin. As controls, none of the proteins could bind to the non-starch substance Sephadex G-10 (Supplemental Figure S15).

Consistent with our previous report (Peng et al., 2014), GST-ISA1 alone was unable to bind to amylopectin (Figure 6, F and G), whereas upon co-incubation with either GST-OsLESV or GST-FLO6, we observed a considerable amount of GST-ISA1 retained in the pellet fraction. It seems that OsLESV exhibits a significantly stronger ability in mediating ISA1 binding to starch than FLO6 (Figure 6, F and G), although both fusion protein themselves showed a similar binding ability to starch, as evidenced by the percentage of protein present in the pellet fraction (Figure 6F; GST-FLO6: 73.37 ± 4.32% versus GST-OsLESV: 71.55 ± 6.23%). Notably, a higher proportion of GST-ISA1 was retained in the pellet fraction in the presence of both GST-OsLESV and GST-FLO6 (Figure 6, F and G). Collectively, these results suggest that OsLESV physically interacts with FLO6 to facilitate ISA1 targeting to starch.

OsLESV genetically interacts with _FLO6_ to regulate starch biosynthesis and endosperm development in rice

To examine the genetic interaction between *OsLESV* and *FLO6*, we identified two new *flo6* and *isa1* mutants and confirmed their defects in endosperm development by iodine staining during late development (Supplemental Figure S16, A and B; Figure 6H). Furthermore, we attempted to cross female *flo6* with male *flo9*, but we were not able to obtain double homozygous mutant plants. We then planted *flo9/FLO9 flo6* and *flo9 flo6/FLO6* heterozygous plants and identified double homozygous mutant grains by genotyping. Notably, double homozygous *flo6 flo9* grains were filled with liquid, and displayed a severely shrunken appearance (Figure 6H). The double mutant had

abolished accumulation of ISA1 protein and obviously reduced levels of PUL and BEI (Figure 6I). The double mutant displayed a dramatic disruption of starch biosynthesis than either single mutant, as evidenced by the measured starch and WSG contents (Supplemental Figure S16C).

We noted that the *flo6 flo9* double mutant exhibits a more severe phenotypic defect than *isa1*, suggesting that both proteins exert some other functions apart from affecting ISA1 targeting to starch granules. To support this notion, we knocked out *OsLESV* or *FLO6* in the *isa1* background to create the *flo9 isa1* and *flo6 isa1* double mutant, respectively (Supplemental Figure S17). It is noted that loss of *ISA1* function did not influence the protein abundance of either OsLESV or FLO6 (Supplemental Figure S17, A–D). As expected, loss-of-function of either gene substantially exaggerated the phenotypic defect of *isa1*, manifested by the more shrunken grain and obviously decreased starch contents (Supplemental Figure S17, E and F). A recent study also reported that the barley (*Hordeum vulgare*) *flo6 isa1* double mutant produced grains with more severe phenotypic defects compared with the *isa1* mutant (Matsushima et al., 2023). Taken together, several lines of genetic evidence suggest that OsLESV and FLO6 indeed exert other function(s) other than targeting ISA1 to starch granules during endosperm development.

Discussion

FLO9 encodes the Arabidopsis LESV homolog OsLESV that functions in ISA1 binding to starch granules in rice endosperm

Amylopectin accounts for up to 75–80% of starch weight; however, the regulatory mechanisms of amylopectin biosynthesis remain obscure. In cereal endosperm, it is thought that amylopectin-synthesizing enzymes such as SSI and BEIIb are delivered to the surfaces of starch granules via their interactions with SSII (Liu et al., 2012). In addition, some starch-synthesizing enzymes/regulators could bind starch granules through their own starch-binding domains, such as the CBM53 domain of AtSS3 and the CBM48 domain of OsBEI (Chaen et al., 2012; Abt et al., 2020). ISA1 is

responsible for removing misplaced branches of amylopectin at the outer edges of starch granules, and its functional loss led to the dramatic accumulation of phytoglycogen instead of amylopectin, suggesting its essential roles in amylopectin biosynthesis (Nakamura et al., 1997; Fujita et al., 2003; Nakagami et al., 2017).

Although a putative CBM48 domain was predicted in rice ISA1 (Du et al., 2018), it appears to be longer than the canonical CBMs (147 amino acids [aa] versus 90–130 aa), and two conserved Trp residues critical for starch binding are mutated (Supplemental Figure S18; Christiansen et al., 2009), likely influencing its starch-binding efficiency. Supporting this hypothesis, our biochemical analysis verified that ISA1 cannot bind directly to starch by itself *in vitro* (Figure 6F; Peng et al., 2014). In rice endosperm, ISA1 is predominantly present as a homo-oligomer, with a small fraction forming a hetero-oligomer with the catalytically inactive ISA2 (Utsumi et al., 2011). Interestingly, ISA2 has been proposed to assist in ISA1 substrate binding in maize (*Zea mays*) and potato (*Solanum tuberosum*) (Hussain et al., 2003; Mehrpouyan et al., 2021). However, the ISA2 loss-of-function mutant exhibited no obvious phenotypic defects in starch biosynthesis of rice endosperm (Utsumi et al., 2011). These findings suggest that plants may have evolved complex mechanisms to facilitate the translocation of ISA1 from the stroma to starch granules, and the molecular machinery by which ISA1 is delivered to starch granules remains to be identified in plants.

Here, we identified *flo9* as an endosperm mutant with a major defect in amylopectin biosynthesis (Figure 1). Notably, apart from its conspicuous opaque phenotype, *flo9* produces endosperm with a hollow core (Figure 1B), which is distinct from other floury endosperm mutants (Bao, 2019; Zhao et al., 2022). The defect in iodine staining in the central region (Figure 1D) together with the amyloplast developmental defects in *flo9* (Figure 2) are most reminiscent of the *isa1* and *sugary-2* rice mutants (Nakamura et al., 1997; Matsushima et al., 2010; Nakagami et al., 2017; Nagamatsu et al., 2022). Although the causal gene responsible for the *sugary-2* phenotype remains unknown, an allelic test showed that *sugary-2* is not

allelic to *isa1* (Nakagami et al., 2017). Our genetic evidence indicates that *flo9* is also not a weak *isa1* allelic mutant; unexpectedly, this causal gene responsible for *flo9* phenotypes encodes a homolog of Arabidopsis LESV (Figure 3; Feike et al., 2016).

Arabidopsis *LESV* is highly expressed in leaves, especially during senescence (http://bar.utoronto.ca/), whereas OsLESV showed substantially higher abundance in developing endosperm, particularly early development (Figure 3G), suggesting that OsLESV plays an important role in starch metabolism in endosperm. In addition, the abundance of OsLESV increased gradually from the exterior to interior of the endosperm (Figure 3, H and I), coinciding with the most affected parts in *flo9* endosperm (Figure 1B). These results suggest that starch biosynthesis in rice endosperm is spatially orchestrated by factors with distinct sub-endosperm accumulation abundance. Supporting this notion, loss-of-function mutation of *FLO7*, which is predominantly expressed in grain periphery, causes a defect in starch synthesis specific in peripheral endosperm (Zhang et al., 2016).

Unlike Arabidopsis PTST1, which transiently binds to starch via the CBM48 domain (Seung et al., 2015), OsLESV could strongly bind to both amylose and amylopectin via its C-terminal Trp-rich region (Figure 4, H–K), resembling Arabidopsis LESV (Feike et al., 2016; Singh et al., 2022; Liu et al., 2023). Mutagenesis of those Trp residues located in OsLESV dramatically abolished its binding to amylopectin (Figure 4L; Supplemental Figure S6, C–E). More strikingly, we found that OsLESV physically interacts with ISA1 via its N-terminal region (Figure 5, A–D). When *ISA1-GFP* was overexpressed in wild-type rice protoplasts, a small proportion of ISA1 was localized to starch granules (Supplemental Figure S12A). This observation could be explained by the presence of endogenous OsLESV protein. Supporting this notion, loss of *OsLESV* function largely impaired the recruitment of ISA1 onto SGs (Figure 5, E and F; Supplemental Figure S12, B–D). Our findings suggest that OsLESV may function as a scaffold protein to help deliver ISA1 onto starch granules.

OsLESV functions cooperatively with FLO6 to regulate starch biosynthesis and endosperm development

FLO6 is identified as a non-enzymatic interacting partner of ISA1 in plants, although its precise function in starch metabolism has been unclear (Peng et al., 2014). *flo6* and *flo9* exhibited a similar defect in starch granule initiation (Figure 2; Peng et al., 2014). Furthermore, we found that either OsLESV or FLO6 depletion influenced the distribution of ISA1 onto starch granules (Figure 5, E and F; Supplemental Figure S13, D and E). These observations indicated that OsLESV and FLO6 might function, at least in part, in a common starch metabolism pathway in rice endosperm. This hypothesis is further supported by the strong physical interaction of OsLESV with FLO6 via their N-terminal regions *in vitro* and *in vivo* (Figure 6, A–C).

Furthermore, the co-expression of OsLESV and FLO6 significantly enhanced the interactions of either protein with ISA1 (Figure 6, D and E; Supplemental Figure S14). An *in vitro* starch binding assay indicated that OsLESV exhibited a stronger ability to bring ISA1 to the proximity of starch granules than FLO6, and that co-incubation of OsLESV and FLO6 had a significantly stronger effect than either protein alone (Figure 6F). Genetically, our evidence showed that loss of both *OsLESV* and *FLO6* functions dramatically disrupted starch biosynthesis, and generated a severely shrunken grain (Figure 6H; Supplemental Figure S16). These results suggested that OsLESV acts synergistically together with FLO6 to control starch biosynthesis and endosperm development.

Based on these findings, we proposed a working model for the role of OsLESV and FLO6 in regulating starch biosynthesis and endosperm development (Figure 7). According to this model, OsLESV and FLO6 are able to recruit ISA1 from the amyloplast stroma through their N-terminal domains. By virtue of the Trp-rich C-terminal domain of OsLESV and the CBM48 domain of FLO6, ISA1 is brought to the surface of starch granules where it is required to remove misplaced starch branches, thereby ensuring the formation of the semi-crystalline amylopectin matrix. Loss of *OsLESV* function considerably compromises the distribution of ISA1 onto

starch granules, whereas loss-of-function mutations of both *OsLESV* and *FLO6* substantially decrease the protein abundance of ISA1, and dramatically disrupted starch biosynthesis and endosperm development.

We also noted the stronger *flo6 flo9* phenotype relative to *isa1* (Figure 6H), suggesting extra function roles of OsLESV and FLO6 in modulating starch synthesis apart from targeting ISA1 to starch granules. Supporting this notion, our genetic evidence showed that either *OsLESV* or *FLO6* genetically interacts with *ISA1* to regulate starch biosynthesis and endosperm development (Supplemental Figure S17). Similar genetic interactions were recently reported for *LESV* and *ISA* in Arabidopsis leaves as well as for *FLO6* and *ISA1* in barley endosperm (Liu et al., 2023; Matsushima et al., 2023). In addition, putative interaction relationships of FLO6 with SSIVb and GBSSI&II were also reported in rice endosperm (Zhang et al., 2022). Based on these findings, we proposed that OsLESV and FLO6 might also target other unknown cargos essential for starch biosynthesis to starch granules during starch biosynthesis.

Why does the targeting of ISA1 onto starch granules require the assistance of multiple proteinaceous non-enzymatic factors? A previous study of rice endosperm suggested that ISA1 can form homohexamers (~530 kD) and hetero-oligomers (~450 kD) (Utsumi and Nakamura, 2006). It is a possible explanation that OsLESV interacts with FLO6 to form a more powerful scaffolding protein complex to efficiently facilitate the delivery of ISA1 homohexamers to starch granules. The more severe phenotypic defect observed in *flo9* than *flo6* suggested that OsLESV might play a more important role than FLO6 in modulating starch biosynthesis and endosperm development. In contrast to those CBM domain-containing enzymes that could directly bind to starch by themselves, such a complex targeting strategy for ISA1 delivery to starch might be more flexible to finely tune starch biosynthesis through maintaining a proper quantity of ISA1 onto starch granules during endosperm development.

Multiple physiological roles of LESV-like proteins in influencing starch

biosynthesis in plants

LESV represents a type of plant-unique protein, and its functional loss generally disrupted the metabolism of both transient and storage starch in plants including Arabidopsis and rice (Feike et al., 2016; Singh et al., 2022; Liu et al., 2023; Figure 1; Supplemental Figure S5). Two functional roles of LESV in starch metabolism have been proposed based on *in vitro* biochemical and genetic data (Singh et al., 2022; Liu et al., 2023). One is the role in modification, in which LESV functions in modulating the glucan structure on the starch granule surface to influence the activity of starch metabolic enzymes (Singh et al., 2022). Another physiological role of Arabidopsis LESV is to help the assembly of amylopectin helices into starch granules (Liu et al., 2023).

In this study, we identified a rice mutant of *OsLESV*, and found that its functional defect dramatically disrupted the biosynthesis of storage starch in endosperm, which is distinguished from starch metabolism in vegetative organs such as leaves. Our combined biochemical, cytological, and genetic evidence pointed to a possible role of LESV-like protein as a scaffolding protein to recruit ISA1 from amyloplast stroma onto starch granule in rice endosperm (Figure 7). Although these possible roles of LESV in modulating starch metabolism appeared to be distinguished from each other, they are not mutually exclusive. We could not rule out the possibility that OsLESV could also influence the glucan structure of the starch granule surface, whereby strengthens the binding of ISA1 to starch granules.

Unexpectedly, we also found that in contrast to FLO6 and ISA1 that accumulated in both the S and LBP fractions (Figure 4G), a considerable amount of OsLESV was present in the TBP fraction (Figure 4G). Intriguingly, OsLESV homologs from Arabidopsis and potato are also found to be encapsulated inside starch granules (Helle et al., 2018; Liu et al., 2023). Consistent with the model proposed for Arabidopsis LESV in amylopectin phase transition (Liu et al., 2023), we found that depletion of OsLESV generated substantial amounts of WSG compared to the wild type (Figure 1E), which is most likely owing to the failure in amylopectin phase transition. Further studies should be aimed to investigate the possible multiple physiological roles of

628 LESV in modulating storage starch metabolism in cereal crops.

Materials and Methods

Plant materials and growth conditions

The *flo9* mutant was isolated from an *N*-methyl-*N*-nitrosourea-induced mutant population of the rice (*Oryza sativa*) *japonica* variety W017. Reciprocal crosses between *flo9* and W017 were used for genetic analysis. An F_2 mapping population was obtained by crossing *flo9* with the *indica* variety Nanjing 11. The *flo6* mutant in the Nipponbare (*japonica*) background and the *isa1* mutant in the Kitaake (*japonica*) background were used in this study. We crossed *flo9* with *flo6* and identified the *flo6 flo9* double mutant by genotyping from the segregated F_2 grains. The primers used for genotyping are listed in Supplemental Data Set S1. Plants were grown in paddy fields under natural conditions or in a greenhouse at the Chinese Academy of Agricultural Sciences, Beijing. Developing seeds at different stages of development were separately collected and frozen in −80°C freezer for use. *Nicotiana benthamiana* plants were grown in a climate chambers at ~21°C for 4 weeks with a 14 h light/10 h dark photoperiod and an illumination intensity of 120–150 μmol m^{-2} s^{-1} using the light-emitting diode (LED) lamps.

Microscopy

For scanning electron microscopy analysis, mature grains were transversely cut with a knife, followed by examination with a HITACHI S-3400N scanning electron microscope (Tokyo, Japan).

For visualization of SGs in developing grains, semi-thin sections were prepared as described previously (Peng et al., 2014). Briefly, transverse sections of the wild-type and *flo9* developing grains at 6, 9 and 12 DAF were fixed in 0.1 M phosphate buffer (pH 7.4) containing 2.5% (v/v) glutaraldehyde for 12 h at 4°C. Fixative samples were dehydrated through a gradient ethanol series (30, 50, 70, 90, and 100% [v/v]), and sequentially embedded in LR White resin (London Resin, 14388-UC). Semi-thin sections (approximately 1 μm in thickness) were prepared with an ultramicrotome

(Leica microsystems, RM2265), and stained with I_2-KI (0.5% [w/v]) or periodic acid-Schiff reagent (PAS; Wu et al., 2016) for 3 min. After washing three times with distilled water, the sections were examined under a Nikon ECLIPSE80i microscope.

For immune-gold electronic microscopy, ultra-thin sections were prepared from high-pressure frozen/freeze-substituted (HPF/FS) samples of *flo9/ProUbi:OsLESV-GFP* transgenic endosperm cells, followed by immunogold labeling as described previously (Ren et al., 2014).

Cell wall labeling was conducted according to a method previously described (Ren et al., 2014). The thick sections (100 μm) prepared from wild-type and *flo9* developing endosperm were stained with Calcofluor white (a non-specific dye for β-glucan, Sigma-Aldrich) at room temperature for 5 min, and washed three times with sodium phosphate (PBS) buffer. Images were taken using a laser scanning confocal microscope (Zeiss LSM980). A 405-nm laser excitation and 475–500-nm prism filter set used for calcofluor white emission. The range of laser intensity was 0.5–3%. Images were taken at 400 Hz, with a picture size of 1024 × 1024 pixels and a below 800 gain score.

Physicochemical properties of rice grains

Soluble and insoluble glucans were prepared from dehulled rice grains as described previously (Nakagami et al., 2017). Total starch, amylose, and WSG contents were enzymatically measured using starch assay kits (Megazyme, K-TSTA-100A), following the manufacturer's protocol. The amylopectin content was calculated as the difference between total starch content and amylose content. Lipid and protein contents of mature grains were determined as described previously (Kang et al., 2005; Liu et al., 2009). The starch pasting properties were determined with a Rapid Visco Analyzer (TecMaster RVA, Perten; Peng et al., 2014). For chain-length distribution (CLD) of total glucans, the sifted rice powder (~0.2 g) was suspended in 10 mL of methanol and boiled for 10 min, followed by centrifugation at 2500*g* for 10 min at room temperature. The resulting precipitate was washed twice with 5 mL of 90% (v/v) methanol to completely remove free sugars. Total glucans were obtained and used to

assess CLD following the methods described previously (Fujita et al., 2003; Peng et al., 2014).

The gelatinization behavior of endosperm starch in urea solution was examined as described previously (Nishi et al., 2001). Briefly, approximately 20 mg of rice powder was separately mixed with 1 mL various concentrated urea solution (0–9 M, pH 6.0) in a 1.5 mL Eppendorf tube. After incubation with shaking at 25°C overnight, the mixture was centrifuged at 8,000*g* for 20 min at room temperature, followed by standing for 1 h. Images were taken with a scanner (Scanmaker 560).

Iodine staining and starch content analysis of leaves

Four-week-old seedlings were grown under a 10-h light/14-h dark diurnal cycle in a climate chamber (HP1500GS; Ruihua, Wuhan, China) at 30°C and 60% relative humidity. Light was provided by fluorescent white-light tubes (400 μmol m^{-2} s^{-1}). For iodine staining, leaves harvested at the end of the day and night were decolourized and stained in Lugol's solution as described previously (Wang et al., 2020). The starch content was determined in the leaves harvested during the diurnal cycle, following the method as described previously (Wang et al., 2020).

Map-based cloning

Floury grains were selected from the F_2 population of *flo9* and Nanjing 11 for preliminary mapping, using over 180 polymorphic simple sequence repeat markers covering the rice genome. To finely map the *OsLESV* locus, new genetic markers were developed by comparing the corresponding genomic sequences of the *japonica* variety Nipponbare and the *indica* variety 93-11 (Supplemental Data Set S1).

Generation of transgenic plants

Full-length coding sequence of *OsLESV* was amplified and cloned into the vector pCUbi1390 (at the HindIII and BamHI sites) driven by its native 1972-bp promoter to generate the *ProOsLESV:OsLESV* construct. GFP with linker sequences was inserted into 30-bp upstream of *OsLESV* stop code to generate OsLESV-GFP fusion under the

control of its native regulatory elements including promoter, intron, and downstream regulatory region, and subsequently integrated into pCAMBIA2300 vector (at the EcoRI and SmaI sites) to generate the *ProOsLESV:gOsLESV*-GFP construct (Ren et al., 2020; Supplemental Figure S7A). Full-length coding sequence of *OsLESV* was cloned into the binary vector pCAMBIA1305-GFP (at the BamHI site) driven by the maize (*Zea mays*) *UBIQUITIN* promoter (Ren et al., 2014) to generate *ProUbi:OsLESV-GFP* construct. To generate *OsLESV* or *FLO6* knockout construct, a 20-bp gene-specific spacer sequence was inserted into the CRISPR-Cas9 expression vector (at the BsaI site) according to a previously described method (Miao et al., 2013).

All above constructs were individually introduced into W017, Kitaake, *flo9* or *isa1* mutant by *Agrobacterium tumefaciens*-mediated transformation (Hiei et al., 1994). Primers were listed in Supplemental Data Set S1.

Phylogenetic analysis

Sequences of *OsLESV* homologs were retrieved from the National Center for Biotechnology Information (NCBI, http://www.ncbi.nlm.nih.gov). The phylogenetic tree was built by the neighbor-joining method (Tamura et al., 2011), using MEGA 5.0 software (http://www.megasoftware.net/). Bootstrap values from 1,000 replicates are given. The amino acid sequences of OsLESV homologs were aligned using ClustalX (Thompson et al., 1994; http://www.clustal.org). The alignment files are provided in Supplemental Files S1 and S2.

Subcellular localization

For subcellular localization of OsLESV and its variants, the full-length and truncations of OsLESV were N terminally fused to GFP in the vector pAN580 (at the XbaI and BamHI sites) to generate the *OsLESV-GFP*, *OsLESV*(ΔcTP^{1-38})*-GFP*, *OsLESV*($\Delta CT^{346-618}$)*-GFP*, *OsLESV*(ΔNT^{39-345})*-GFP*, and *OsLESV*(ΔNT^{39-345})*;(16W-16A)-GFP* constructs, respectively. The sequence of the OsLESV(ΔNT^{39-345});(16W-16A) was synthesized in GeneScript Biotech (Nanjing

China; https://www.genscript.com.cn/). Full-length coding sequence of *GBSSII* was cloned into the pAN583 vector (at the XbaI and BamHI sites) with a mCherry fluorescent tag and used as a SG marker (Dian et al., 2003). These transient expression constructs were introduced into rice protoplasts following a PEG-mediated transfection method (Chen et al., 2006). Confocal imaging was performed using a laser scanning confocal microscope (Zeiss LSM980). For GFP observations, the excitation laser wavelength was set at 488 nm, and the emission laser was collected at 495–550 nm. For mCherry observations, the excitation laser wavelength was set at 561 nm, and the emission laser was collected at 570–620 nm. The range of laser intensity was 0.5–3%. Images were taken at 400 Hz, with a picture size of 1024 × 1024 pixels and a below 800 gain score.

Glucan-binding assay

Glucan binding assays were performed *in vitro* following previous methods with minor modifications (Kerk et al., 2006; Lohmeier-Vogel et al., 2008; Peng et al., 2014). Full-length coding sequences of *OsLESV*, *FLO6*, and *ISA1*, as well as *OsLESV* variants were separately cloned into the pGEX4T-2 vector (at the EcoRI and BamHI sites; GE Healthcare). The expression of recombinant protein and free glutathione-S-transferase (GST) was induced in *Escherichia coli* BL21 (DE3) cells with 0.5 mM isopropyl β-D-thiogalactopyranoside (IPTG) at 16°C for 18 h, and then purification was performed with GST beads (Beaver; 70601-100) according to the manufacturer's instructions. Recombinant proteins (~1 μg) were separately incubated with excess amylopectin (~30 mg; Sigma-Aldrich, St. Louis, MO, USA), or amylose (~30 mg; type III; Sigma-Aldrich) suspended in a binding buffer (50 mM HEPES-NaOH [pH 7.4], 2 mM $MgCl_2$, 1 mM DTT, 0.1% [w/v] BSA, and 0.01% [v/v] Triton X-100) with a total volume of 250 μL, by mixing end-over-end for 30 min at 20°C. The unbound fraction was collected in the supernatant by centrifugation at 5,000*g* for 30 s. The pellets were washed three times with the binding buffer, and re-suspended in 250 μL of elution buffer (50 mM HEPES-NaOH, pH 7.4, 2 mM $MgCl_2$, 1 mM DTT, and 4% [v/v] SDS) as the bound fraction. Sephadex G-10 beads

(Sigma-Aldrich), a non-starch substance was used as a negative control (Abt et al., 2020; David et al., 2022). The unbound and bound fractions were subject to SDS-PAGE, followed by immunoblotting using anti-GST antibodies.

For *in vitro* starch binding assays with different protein combinations, 1 μg of each recombinant protein in different combinations was incubated with excess amylopectin (~100 mg) in the binding buffer in a total volume of 500 μL. The subsequent procedures were performed as described above. Proteins in different fractions were detected by SDS-PAGE, followed by immunoblotting using anti-OsLESV, anti-FLO6, and anti-ISA1 antibodies. Free GST protein was used as a negative control. Sephadex G-10 beads were also used as a non-starch control for non-specific binding or for protein precipitation. Each experiment was performed three times independently with similar results.

Far-UV Circular dichroism (CD) spectroscopy

The CD spectra of recombinant GST-OsLESV-CT (as control) and GST-OsLESV-CT(16W-16A) proteins were examined at 25°C in PBS buffer at a concentration of 0.2 mg/mL with a JASCO J-710 spectropolarimeter (Tokyo, Japan). Path length of the cell was 1 mm. Recombinant protein concentration was evaluated from absorption measurements at 280 nm using a double-beam λ-25 spectrophotometer (Perkin Elmer, Norwalk, CT, USA). CD spectra and molar ellipticity were obtained over the wavelength range of 200–260 nm. The results are indicated by mean residue ellipticity [θ] MRW.

Antibodies

Polyclonal antibodies against starch-synthesizing enzymes, including ADP-glucose pyrophosphorylase (AGPase) subunits (AGPS2b and AGPL2, dilution 1:2000), SSIIa (dilution 1:1000), BEI (dilution 1:3000), BEIIb (dilution 1:3000), phosphorylase 1 (PHO1, dilution 1:3000), and GBSSI (dilution 1:5000), were produced in rabbits at Yingji Biotech (http:// www.immunogen.com.cn/) as described previously (Long et al., 2018).

To produce polyclonal antibodies against OsLESV, FLO6, and ISA1, we cloned partial coding sequences of OsLESV(amino acids 1 to 190), FLO6 (amino acids 95 to 240), and ISA1 (amino acids 103 to 429) into pET-28a expression vector (at the EcoRI and BamHI sites; Novagen) for recombinant protein productions. After purification using the His beads (Beaver; 70501-100), approximately 1 mg of each recombination protein was obtained and injected into rabbits for polyclonal antibodies production at ABclonal biotechnology (Wuhan, China; https://abclonal.com.cn/). These antibodies were diluted at 1:2000. Anti-actin (Abmart, M20009L), anti-GST (MBL, PM013-7), anti-His (MBL, D291-7), anti-GFP (Roche, 11814460001), anti-HA (MBL, M180-7), anti-cMYC (MBL, M192-7), and anti-Flag (Sigma, A8592) antibodies are commercially available and diluted at 1:5000.

Protein extraction and immunoblotting

Total proteins were extracted from the developing endosperm samples or mature grains, and subject to immunoblot analysis (Wang et al., 2010; Ren et al., 2020). Briefly, developing rice grains were dehulled and homogenized in an ice-cold lysis buffer (50 mM Tris-MES, pH 7.5, 1 mM $MgCl_2$, 0.5 M sucrose, 10 mM EDTA, 5 mM DTT, 0.1% [v/v] Nonidet P-40, and 1× Complete Protease Inhibitor Cocktail [Roche]) in tissue:buffer ratio of 1:20 (w/v). After incubation for 2 h at 4°C with shaking, the supernatant was collected by centrifugation at 12,000*g* for further analyses.

The fractioned rice powder from mature grains was prepared as previously described (Takahashi et al., 2019). Briefly, ~10 g of brown rice was polished to 90% (w/w) of the original weight by removing embryo, pericarp, and aleurone layer using a rice polisher (KETT, Japan). The resulting polished rice (~9 g) was further polished to 70%, 50%, and 30% of the original weight (~10 g), respectively. Rice powder was sampled at each step, namely 90–70%, 70–50%, and 50–30% rice powder. The remaining polished rice (~3 g) was ground into flour using a sample mill (FOSS, CT410) and sampled as 30–0% rice powder. Total protein extraction and immunoblot analysis were performed as described above with modification in the lysis buffer (4%

SDS [w/v], 4 M urea, 5% [v/v] β-mercaptoethanol, and 125 mM Tris-HCl [pH 6.8]).

The soluble protein, the SG loosely bound protein, and the SG tightly bound protein were extracted from the wild-type, *flo9*, and *flo6* developing endosperm (9 DAF), as described previously (Fujita et al., 2006) with minor modifications. Approximately 0.1 g of developing endosperm was homogenized in 500 μL buffer A (50 mM Tris-HCl [pH 7.5], 8 mM $MgCl_2$, 12.5% [v/v] glycerol, and Protease Inhibitor Cocktail [Roche]). After centrifugation, the supernatant was used as the soluble fraction. The loosely and tightly bound fractions were prepared from the residual pellet as described previously (Fujita et al. 2006). Three independent experiments were performed. The integrated density of protein bands was calculated by the Image J software (https://imagej.nih.gov/ij/). Antibodies against ISA1, OsLESV, FLO6, FLO4, BEI, and GBSSI were used for detection.

RNA extraction and RT-qPCR analysis

Total RNA was isolated from various tissues using a ZR Plant RNA MiniPrep Kit (ZYMO Research, Irvine, California, USA) following the manufacturer's protocol. First-strand cDNA was synthesized from 2 μg of total RNA with a QuantiTect reverse transcription kit (Qiagen, Hilden, Germany) following the manufacturer's protocol. RT-qPCR was performed on an ABI prism 7500 Real-Time PCR System using an SYBR premix Ex Taq Kit (TaKaRa) with rice *ACTIN I* gene as an internal control. The relative expression level was normalized from three biological replicates data via $2^{-\triangle\triangle Ct}$ method (Livak and Schmittgen, 2001). The primers are listed in Supplemental Data Set S1.

Protein-protein interaction assays

For Y2H assays, full-length or truncated coding sequences of *OsLESV*, *FLO6*, and *ISA1* were separately cloned into both pGADT7 and pGBKT7 vectors using an infusion cloning kit (at the EcoRI and BamHI sites; Clontech). Various combinations of plasmids were cotransformed into yeast (*Saccharomyces cerevisiae*) strain AH109, followed by incubation and interaction screening according to the manufacturer's

protocols (Clontech). Yeast soluble proteins were extracted following yeast protocols handbook (Clontech). Briefly, cell pellets collected from overnight liquid cultures were resuspended in 100 μL (per 7.5 OD_{600} units of cells) of ice-cold TCA buffer (20 mM Tris-HCl, [pH 8.0], 50 mM Ammonium acetate, 2 mM EDTA, Protease Inhibitor Cocktail [Roche]). Each cell suspension was transferred into a fresh 1.5-mL centrifuge tube containing 100 μL of acid-washed glass beads (425–600 mm; Sigma #G-8772) and homogenized by a Bead-Beater at the highest speed for 10 min with cooling at intervals. Transfer the supernatant above the settled glass beads to fresh 1.5-mL ice-cold centrifuge tubes. The residual unbroken cells were disrupted again. Soluble proteins were collected from combined supernatant by centrifugation at 15,000*g* for 10 min at 4°C. Protein concentration was quantified by a Bradford-based protein assay (Bio-Rad) reagent (http://www.bio-rad.com), and ~15 μg of each sample was loaded onto the SDS-PAGE gel.

For pull-down assays, the full-length coding sequences of *FLO6* and *ISA1* were separately cloned into the vector pET30a (at the EcoRI and BamHI sites; Novagen) to generate the *His-FLO6* and *His-ISA1* constructs, respectively. The recombinant proteins were purified using the His beads (Beaver; 70501-100), according to the manufacturer's instructions. Equal amounts (2 μg) of GST and GST-OsLESV were separately incubated with 20 μL of GST beads (Beaver; 70601-100) in 1 mL of binding buffer (50 mM Tris-HCl [pH 7.5], 100 mM NaCl, 0.5% [v/v] Triton X-100, and Protease Inhibitor Cocktail [Roche]) at 4°C for 1 h with gentle rotation. Approximately 2 μg of purified His-tagged FLO6 or ISA1 combination protein was added and incubated for another 2 h. The beads were washed at least three times with the binding buffer. Eluted proteins were separated by SDS-PAGE and detected by anti-GST (dilution 1:5000) and anti-His (dilution 1:5000) antibodies.

For yeast three-hybrid assay, full-length coding sequence of *ISA1* was cloned into the pGADT7 vector (at the EcoRI and BamHI sites; Clontech) to generate AD-ISA1, and both full-length coding sequences of *FLO6* and *OsLESV* were cloned into the pBridge vector (at the EcoRI and BamHI sites; Clontech) to generate *FLO6-OsLESV-pBridge* or *OsLESV-FLO6-pBridge* constructs, respectively. Yeast

898 transformation and screening was conducted as described in Y2H. β-galactosidase
899 activity was measured by a liquid culture assay using chlorophenol
900 red-β-D-galactopyranoside (CPRG) following the manufacturer's protocols
901 (Clontech).

902 For LCI assays, the full-length coding sequences of *OsLESV*, *FLO6*, *ISA3*, and
903 *FLO7* were cloned into the pCAMBIA-nLUC vector (at the KpnI and SalI sites; Chen
904 et al., 2008) to generate OsLESV-nLUC, FLO6-nLUC, ISA3-nLUC, and
905 FLO7-nLUC, respectively. The coding sequences of *ISA1*, *FLO6*, *ISA3*, and *FLO7*
906 were cloned into the pCAMBIA-cLUC vector (at the SacI site; Chen et al., 2008) to
907 generate ISA1-cLUC, FLO6-cLUC, ISA3-cLUC, and FLO7-cLUC, respectively. All
908 constructs were introduced into *Agrobacterium tumefaciens* strain EHA105. Various
909 combinations of strains were co-infiltrated into *N. benthamiana* leaves as described
910 previously (Waadt and Kudla, 2008). After 2–3 days, the relative LUC activity was
911 measured by Tanon-5200 chemiluminescent imaging system (Tanon science and
912 technology), as described previously (Chen et al., 2008). ISA3 and FLO7 act as
913 negative controls for the assays.

914 For *in vivo* CoIP assay, full-length coding sequence of *OsLESV* was cloned into the
915 pCAMBIA1305-GFP vector (at the XbaI and BamHI sites; Ren et al., 2014) to
916 generate OsLESV-GFP. Full-length coding sequence of *ISA1* was cloned into
917 pCAMBIA1300-221-Flag vector (at the KpnI and BamHI sites; Ren et al., 2014) to
918 generate ISA1-Flag. Various combinations of plasmids were transiently co-expressed
919 in rice protoplasts as previously described (Chen et al., 2006). After incubation
920 overnight, total protein was extracted from protoplasts with 500 μL of ice-cold protein
921 extraction buffer (50 mM Tris-HCl [pH 7.5], 150 mM NaCl, 10 mM $MgCl_2$, 1 mM
922 EDTA, 5 mM DTT, 0.1% [v/v] Nonidet P-40, 10% [v/v] glycerol, and Protease
923 Inhibitor Cocktail [Roche]), followed by incubation with 20 μL of anti-GFP
924 mAb-Magnetic beads (MBL, D153-10) for 1 h at 4°C with shaking. The beads were
925 washed three times with extraction buffer, and the bound protein was eluted with a
926 reducing buffer, followed by SDS-PAGE and immunoblotting using anti-GFP
927 (dilution 1:5000) and anti-Flag (dilution 1:5000) antibodies.

Statistical Analysis

The statistical results are indicated as means ± SD, where *n* represents the number of biological replicates. GraphPad Prism 5.0 and statistical software SPSS 13.0 (SPSS) were used for statistical analysis. Detailed statistical analysis data are provided as Supplemental Data Set S2.

Accession numbers

Sequence data from this article can be found in the GenBank/EMBL libraries under the following accession numbers: OsLESV (Os11g0586300), FLO6 (Os03g0686900), ISA1 (Os08g0520900), GBSSI (Os06g0133000), GBSSII (Os07g0412100), PUL (Os04g0164900), PHO1 (Os03g0758100), AGPS2b (Os08g0345800), AGPL2 (Os01g0633100), SSI (Os06g0160700), SSIIa (Os06g0229800), BEI (Os06g0726400), BEIIb (Os02g0528200), and FLO4 (Os05g0405000). Accession numbers for the sequences used in phylogenetic tree constructed were listed on the tree.

Funding information

This work was supported by grants from the National Key Research and Development Program of China (2021YFF1000200), National Natural Science Foundation of China (31830064, 91935301, and 32001518), Innovation Program of Chinese Academy of Agricultural Sciences, International Science & Technology Innovation Program of Chinese Academy of Agricultural Sciences (CAAS-ZDRW202109), Natural Science Foundation of Jiangsu Province, Major Project (BK20212010), and Jiangsu Science and Technology Development Program (BE2021359). This work was also supported by the Central Public-Interest Scientific Institution Basal Research Fund, China (Y2021YJ18).

Conflict of interest statement. The authors declare no conflict of interests.

Acknowledgments

We thank the Core Facility Platform, Institute of Crop Sciences, Chinese Academy of Agricultural Science, for their assistance with confocal imaging and transmission electron microscopy analysis. We also thank Jiangsu Nanjing Rice Germplasm Resources National Field Observation and Research Station for careful field management.

Author contributions

J.W., Y.R., and W.Z. designed the research; H.Y., W.Z., and Y.W. performed most of the experiments. J.J. screened the *flo9* mutant material and cloned the gene; Y.Z. constructed the GFP-fused genomic complementation vector; Y.W., Y.F., Z.S., H.X., X.L., Y.X.W., X.H., W.X.Z., and C.Z. generated the transgenic plants and planted the rice materials; X.Z. performed some transgenic experiments; X.W., X.T., R.W., J.Z., Y.C., X.Y., J.C., X.G., J.X., L.J., S.L., C.L., X.Z., and H.W. provided technical assistance; H.Y., Y.R., and W.Z. analyzed the data and wrote the article.

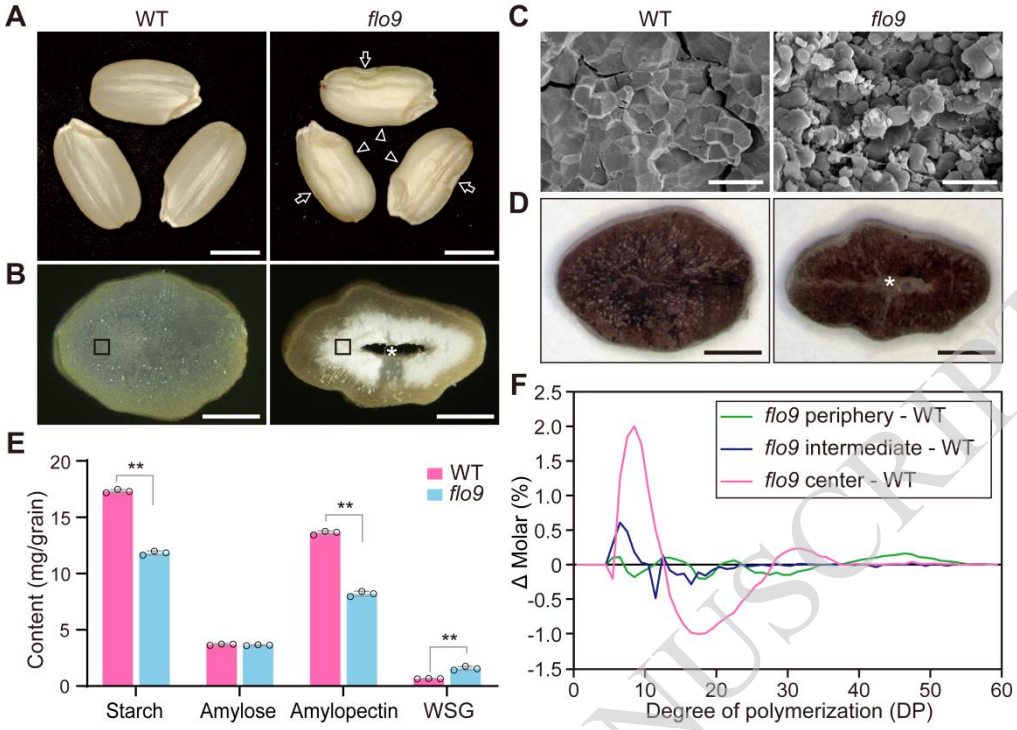

Figure 1. Phenotypic characterization of the *flo9* mutant.

A, Comparison of the representative wild-type (WT) and *flo9* mature grains. Bars = 2 mm. Arrows and arrowheads indicate dimpled indentations and constrictions at the dorsal and ventral sides, respectively.

B, Transverse sections of the representative WT and *flo9* mature grains. Bars = 1 mm. Asterisk indicates the hollow core.

C, Comparison of starch grains (SGs) observed via scanning electron microscope in magnified regions of WT and *flo9* indicated by black squares in (B). Bars = 20 μm.

D, Iodine-stained transverse sections of the representative WT and *flo9* maturing grains at 25 days after flowering (DAF). Bars = 1 mm. Asterisk indicates the hardly-stained core.

E, Determination of total starch, amylose, amylopectin, and water-soluble-glucan (WSG) contents of WT and *flo9* mature grains. Values are means ± SD. $^{**}P < 0.01$ by Student's *t*-test ($n = 3$).

F, Differences in chain length distribution (CLD) patterns of total glucans between WT and *flo9*. Note that rice powder collected from the periphery, intermediate, and center of grains were separately used to determine the glucan CLD.

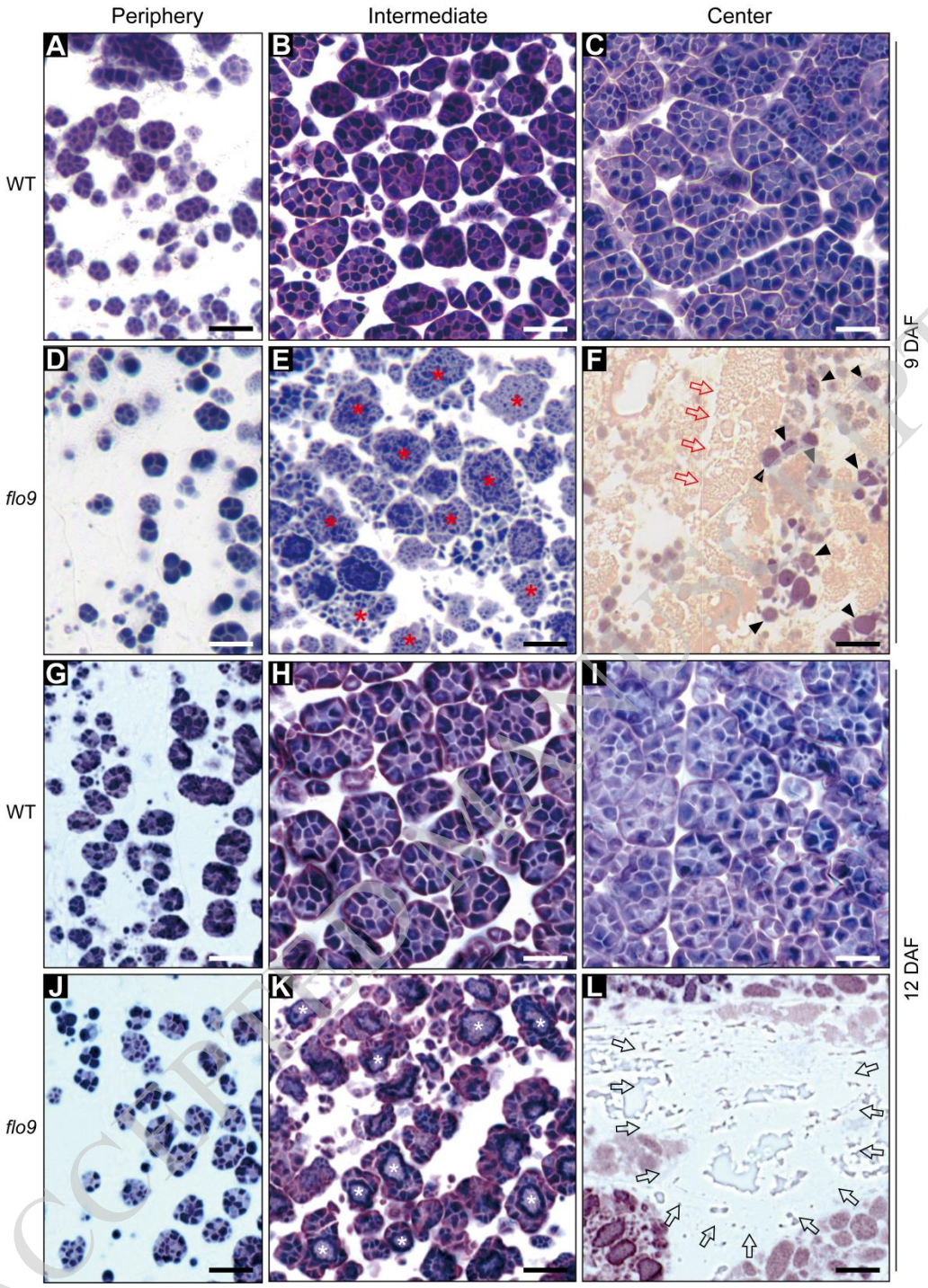

Figure 2. Defects in starch grain (SG) initiation of *flo9* grains.

A–L, Comparison of SGs from iodine-stained semi-thin sections prepared from developing wild-type (WT) and *flo9* endosperm at 9 days after flowering (DAF; A–F) and 12 DAF (G–L). Periphery, intermediate, and center indicate the translucent, floury-white, and hollow regions of *flo9* endosperm, respectively, and the corresponding regions of the WT. Red asterisks in (E) indicate abnormal amyloplasts containing tiny granules. Black arrowheads in (F) indicate atypical

amyloplasts stained weakly with iodine and lacking compound structure. Red arrows in (F) indicate the amorphous SGs filled with pink-stained phytoglycogen-like substances. White asterisks in (K) indicate the amorphous structures with a dark-stained edge in *flo9* amyloplasts. Arrows in (L) outline the contiguous region that is not stained by iodine. Bars = 10 μm.

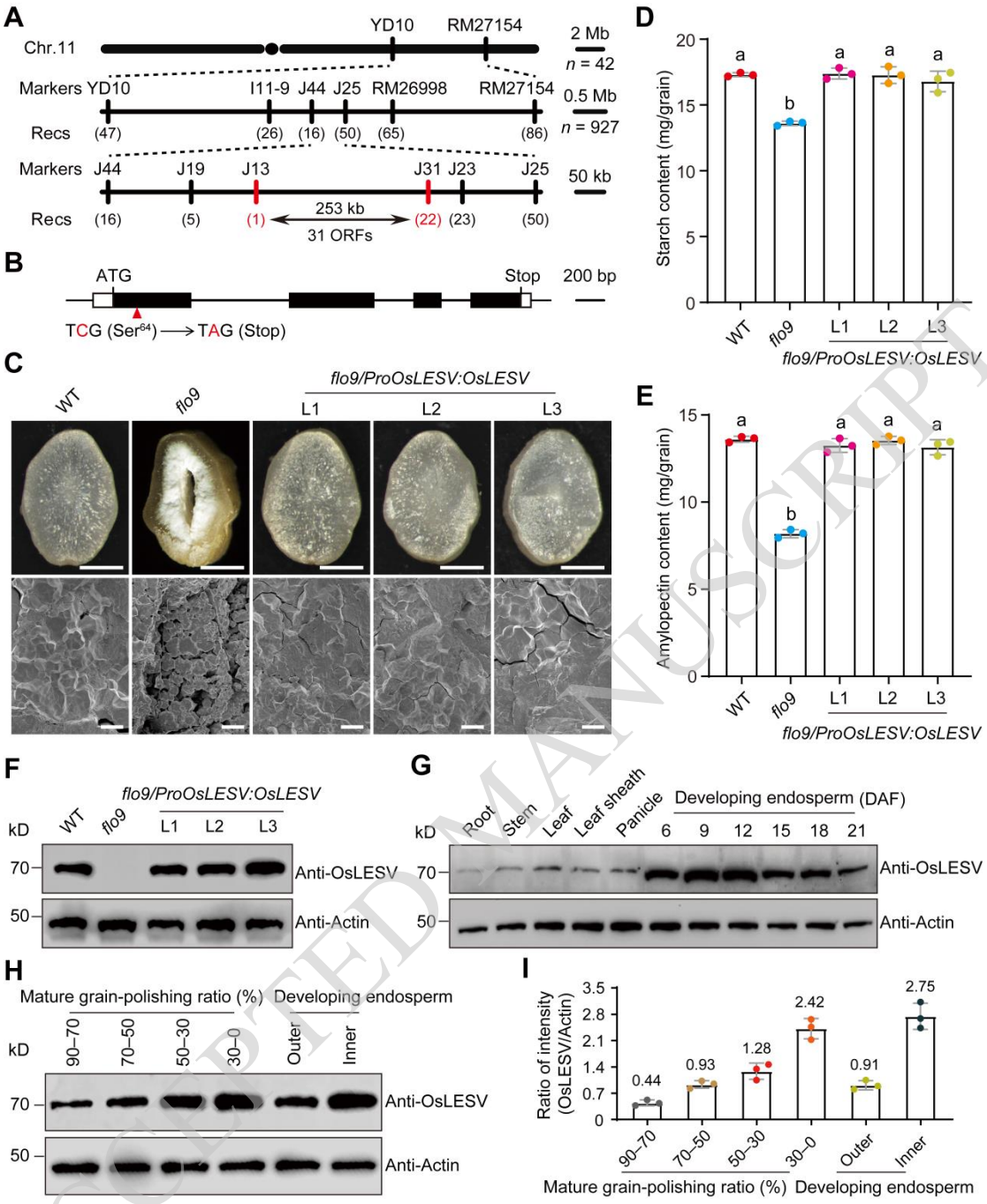

Figure 3. Map-based cloning of the *OsLESV* gene and expression pattern of the OsLESV protein.

A, Fine mapping of the *OsLESV* locus. The *OsLESV* locus was located to a 253-kb region between markers J13 and J31 (red vertical lines). Numbers of recombinants and molecular markers are shown. Chr., chromosome; ORFs, open reading frames; Recs, recombinants.

B, Genomic structure and the mutation site of *OsLESV*. A single nucleotide substitution in the first exon of *OsLESV* led to a premature stop codon in *flo9*. Red arrowhead indicates the mutation site in *flo9*.

C, Expression of the *OsLESV* gene driven by its native promoter restored the grain appearance

(the upper panel) and starch grain (SG) morphology (the lower panel). L1 to L3 indicate three independent T_4 generation transgenic lines. Bars in the upper panel = 1 mm; bars in the lower panel = 10 μm. WT, wild type.

D and E, Determination of total starch (D) and amylopectin (E) contents in mature grains of WT, *flo9*, and complemented transgenic lines. Values are means ± SD. $P < 0.05$ by Duncan's multiple range tests ($n = 3$).

F, OsLESV antibodies specifically recognize the endogenous OsLESV protein in total protein extracts of mature grains from WT and complemented transgenic lines but not in *flo9*. Anti-actin antibody was used as a loading control.

G, Protein accumulation profiles of OsLESV in various tissues and different developmental stages of endosperm. DAF, days after flowering. Anti-actin antibody was used as a loading control.

H, Immunoblot analysis of the spatial distribution of OsLESV within endosperm using total protein extracts from different portions of mature grain and developing endosperm by the OsLESV antibodies. Mature grain-polishing ratio refers to the ratio (w/w) of polished rice to the brown rice. Brown rice was sequentially polished to 90%, 70%, 50%, 30% (w/w) of its original weight (approximately 10 g). Rice powder produced at each polishing step was collected as samples with a 90–70%, 70–50%, or 50–30% of grain-polishing ratio. The gradient decrease of grain-polishing ratio indicated that samples were collected from the exterior to the interior of rice endosperm, thus representing the periphery, intermediate, and center of the endosperm, respectively. Anti-actin antibody was used as a loading control. Three independent experiments were performed.

I, Quantification of OsLESV protein in different fractions of (H). The intensity of OsLESV was normalized by the loading control of anti-actin antibody using the Image J software. Values are means ± SD ($n = 3$). The average values were shown on the corresponding columns.

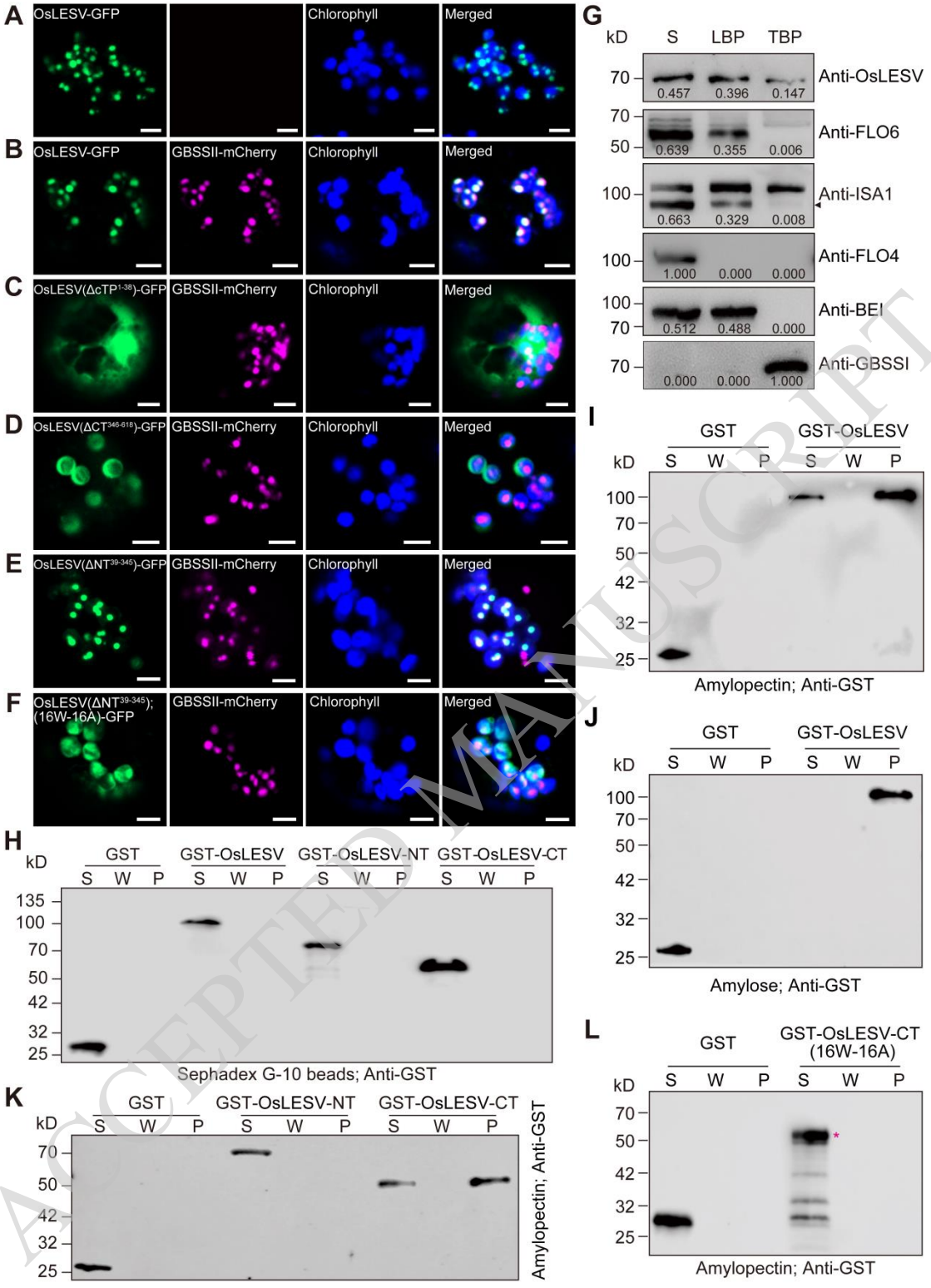

Figure 4. OsLESV binds to starch *in vivo* and *in vitro*.

A, Representative confocal microscopy images showing that OsLESV-GFP is localized to disc-like structures within chloroplasts of rice protoplasts. Blue signals are autofluorescence from chlorophylls in chloroplasts. The rightmost panel represents the merged image of GFP, mCherry, and chlorophyll fluorescence signals. Bars = 5 μm.

B, Representative confocal microscopy images showing that OsLESV-GFP colocalizes with GBSSII-mCherry within chloroplasts of rice protoplasts. Bars = 5 μm.

C–E, Different deletions or mutations of OsLESV-GFP fusion vectors were transiently co-expressed with GBSSII-mCherry in rice protoplasts, respectively. Note that OsLESV(ΔCT$^{346-618}$)-GFP lacking the C-terminal tryptophan (Trp)-rich region displayed a stromal localization pattern, whereas OsLESV(ΔNT$^{39-345}$)-GFP was tightly associated with GBSSII-mCherry within chloroplasts. cTP, chloroplast transit peptide; CT and NT separately indicate the C and N termini of OsLESV. Bars = 5 μm.

F, Representative confocal microscopy images showing that OsLESV(ΔNT$^{39-345}$)-GFP with mutations of 16 evolutionarily conserved Trp to Ala residues abolished its colocalization with starch grains (SGs). NT, N terminus of OsLESV; 16W-16A, the mutation of 16 evolutionarily conserved tryptophan (W) residues to alanine (A) in the tryptophan-rich region of OsLESV. Bars = 5 μm.

G, Association of OsLESV with starch in developing wild-type (WT) endosperm (9 days after flowering). FLO4 (a cytosolic protein), BEI (a granule-associated protein), and GBSSI (a granule-bound protein) were used as marker proteins for different fractions. The volume of each sample subject to SDS-PAGE was 10 μL. LBP, the loosely bound protein; S, the soluble protein; TBP, the tightly bound protein. Arrowhead indicates the target band of ISA1. The relative band intensity of proteins was calculated by image J software. Three independent experiments were performed.

H–J, Binding of recombinant GST-OsLESV protein or its variants to Sephadex G-10 beads (H), amylopectin (I), and amylose (J) *in vitro*. CT and NT separately indicate the C and N termini of OsLESV; GST, glutathione S-transferase; P, the pellet; S, the soluble fraction; W, the final wash.

K, GST-OsLESV-CT recombinant protein but not GST-OsLESV-NT protein specifically bound to amylopectin *in vitro*. CT and NT separately indicate the C and N termini of OsLESV; GST, glutathione S-transferase; P, the pellet; S, the soluble fraction; W, the final wash.

L, Mutations of evolutionarily conserved tryptophan Trp residues in the GST-OsLESV-CT recombinant protein abolished its binding to amylopectin *in vitro*. Equivalent volume (10 μL) of each sample was loaded in (H–L). Asterisk indicates target band of GST-OsLESV-CT(16W-16A) recombinant protein. CT, C terminus of OsLESV. GST, glutathione S-transferase; P, the pellet; S, the soluble fraction; W, the final wash. 16W-16A indicates the mutation of 16 conserved tryptophan (W) residues to alanine (A).

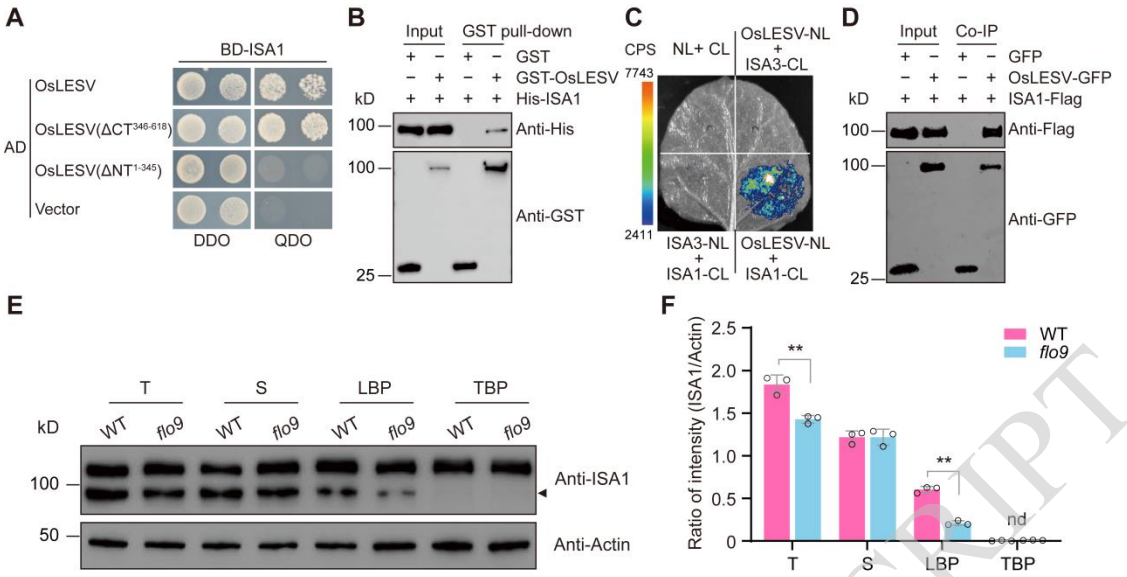

Figure 5. OsLESV physically interacts with ISA1**.**

A, Y2H assay showing that full-length OsLESV and its N terminus interact with ISA1. AD, activation domain; BD, binding domain; CT and NT separately indicate the C and N termini of OsLESV; DDO, control medium (SD/-Trp-Leu); QDO, selective medium (SD/-Trp-Leu-His-Ade). The empty pGADT7 vector was used as a negative control.

B, *In vitro* GST pull-down assay showing that glutathione S-transferase (GST)-tagged OsLESV but not free GST tag could pull down His-tagged ISA1. The symbols "+" or "-" indicates the presence or absence of the corresponding protein.

C, LCI assay showing that OsLESV can specifically interact with ISA1 in *N. benthamiana* leaf epidermal cells. ISA3 was used as a negative control. Colored scale bar indicates the luminescence intensity in counts per second (CPS). NL, N terminus of LUC; CL, C terminus of LUC.

D, CoIP assay verified the interaction between OsLESV and ISA1 in rice protoplasts. ISA1-Flag was transiently coexpressed in rice protoplasts with OsLESV-GFP or free GFP, respectively. ISA1-Flag could be coimmunoprecipitated by OsLESV-GFP but not free GFP using anti-GFP magnetic beads. The symbols "+" or "-" indicates the presence or absence of the corresponding protein.

E, Immunoblot analysis of total ISA1 and its starch association in wild-type (WT) and *flo9* developing endosperm (9 days after flowering). Anti-actin antibody was used as a loading control. The arrowhead indicates the ISA1 band. T, the total protein; LBP, the loosely bound protein; S, the soluble fraction; TBP, the tightly bound protein. Three independent experiments were performed.

F, Quantification of ISA1 protein level in (E). The intensity of ISA1 was normalized by the corresponding intensity of anti-actin antibody using the Image J software. nd, no detection. Values are means ± SD. $^{**}P < 0.01$ by Student's *t*-test ($n = 3$).

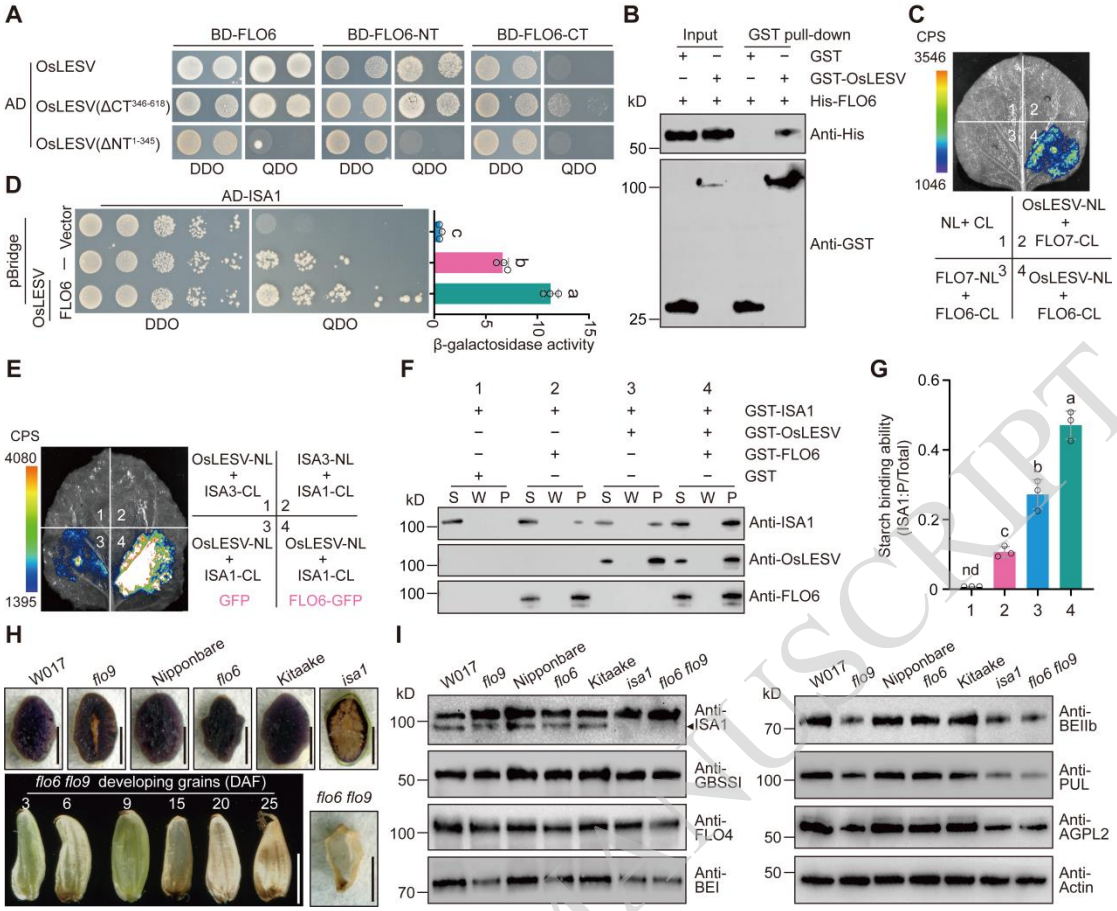

Figure 6. OsLESV physically interacts with FLO6 through their N termini.

A, Y2H analysis showing that OsLESV and FLO6 interact with each other via their N termini. AD, activation domain; BD, binding domain; CT and NT separately indicate the C and N termini of OsLESV or FLO6; DDO, control medium (SD/-Trp-Leu); QDO, selective medium (SD/-Trp-Leu-His-Ade).

B, *In vitro* GST pull-down assay showing that glutathione S-transferase (GST)-tagged OsLESV but not free GST can pull down His-tagged FLO6. The symbols "+" or "-" indicates the presence or absence of the corresponding protein.

C, LCI assay showing that OsLESV can interact with ISA1 in *N. benthamiana* leaf epidermal cells. Chloroplast-localized FLO7 was used as a negative control. Colored scale bar indicates the luminescence intensity in counts per second (CPS). NL, N terminus of LUC; CL, C terminus of LUC.

D, Yeast three-hybrid assay showing that FLO6 can enhance the interaction between OsLESV and ISA1. Note that full-length coding sequence of *OsLESV* was fused to binding domain (MCS I: multiple cloning site I) and driven by constitutive *ADH1* promoter, whereas *FLO6* was inserted

into MCS II and driven by a Met-responsive promoter. β-galactosidase activity was measured using CPRG as substrate. Values are means ± SD. $P < 0.05$ by Duncan's multiple range tests (n = 3). AD, activation domain; DDO, control medium (SD/-Trp-Leu); QDO, selective medium (SD/-Trp-Leu-His-Ade).

E, LCI assays showing that the FLO6-GFP fusion protein but not free GFP can promote the interaction of OsLESV with ISA1. ISA3 was used as a negative control. Colored scale bar indicates the luminescence intensity in counts per second (CPS). NL, N terminus of LUC; CL, C terminus of LUC.

F, Effects of OsLESV and FLO6 on ISA1 binding to amylopectin *in vitro*. Equal amount of each recombinant protein was combined as indicated and co-incubated with amylopectin for 30 min. Amylopectin was pelleted by centrifugation. Proteins in the supernatant (S), the final wash (W), and the pellet (P) were subject to immunoblot analyses using anti-OsLESV, anti-FLO6, and anti-ISA1 antibodies, respectively. Equivalent volume (10 μL) of each sample was loaded. Three independent experiments were performed. The symbols "+" or "-" indicates the presence or absence of the corresponding protein.

G, Quantification of the ISA1 protein binding to amylopectin in (F). The percentage of starch-binding ISA1 in total ISA1 (S+W+P) was quantified with the Image J software. Values are means ± SD. $P < 0.05$ by Duncan's multiple range tests (n = 3). nd, no detection.

H, Phenotypic analyses of the *flo6 flo9* double mutant. Top panel: Iodine-stained transverse-sections of developing grains of W017 (wild type for *flo9*), *flo9*, Nipponbare (wild type for *flo6*), *flo6*, Kitaake (wild type for *isa1*), and *isa1* at 25 DAF. Bottom panel: The left shows the developing *flo6 flo9* caryopsis from 3 to 25 days after flowering (DAF) (numbers above denote the DAF). Note that the core region of *flo9* as well as most of the *isa1* endosperm were not stained by iodine. The right shows a transverse-section of the *flo6 flo9* grain at 25 DAF. Bars = 2 mm.

I, Immunoblot analysis of starch synthesis-related enzymes protein abundance in total protein extracts of developing endosperm of the *flo9*, *flo6*, and *isa1* single mutant, and their corresponding wild type, as well as the double mutant *flo6 flo9* at 25 DAF. Anti-actin antibody was used as a loading control. The arrowhead indicates the band of ISA1.

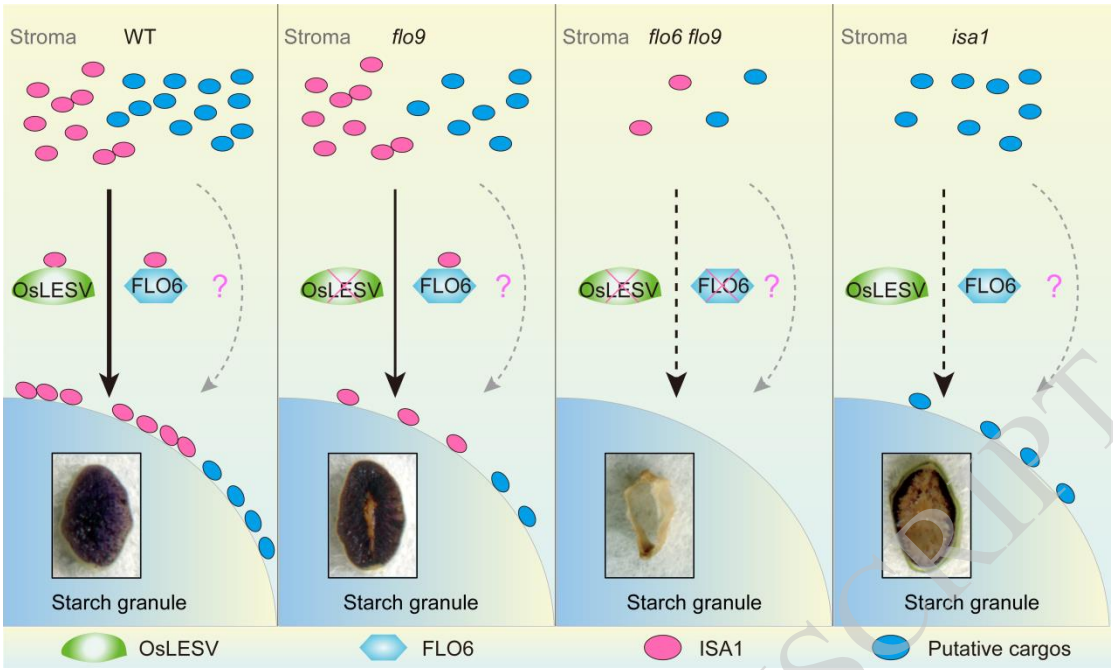

Figure 7. Working model for the OsLESV-FLO6 molecular module in facilitating ISA1 binding to starch granules in rice endosperm.

In the wild-type (WT) endosperm, OsLESV and FLO6 form a functional protein complex to recruit ISA1 from the stroma to starch granules, where ISA1 is responsible for the removal of misplaced branches in amylopectin. Loss of *OsLESV* function considerably compromises the distribution of ISA1 onto starch granules, whereas loss-of-function mutations of both *OsLESV* and *FLO6* substantially decreased the protein abundance of ISA1, and dramatically disrupted starch biosynthesis and endosperm development. Loss of *ISA1* function accumulates large amounts of phytoglycogen instead of starch, and thus disrupts the formation of higher-order amylopectin structure and amylopectin crystallizing. The thick solid arrow indicates an effective targeting of ISA1 to starch granules, while the thin solid arrow and dashed black arrows indicate weak and disturbed binding of ISA1 to starch granules, respectively. In addition, the dotted grey arrow indicates a possible functional role of OsLESV and FLO6 in the delivery of other unknown cargos onto starch granules during starch biosynthesis. Insets inside of starch granule model denote the I_2-KI staining of transverse sections of corresponding grains.

References

Abt MR, Pfister B, Sharma M, Eicke S, Burgy L, Neale I, Seung D, Zeeman SC (2020) STARCH SYNTHASE5, a noncanonical starch synthase-like protein, promotes starch granule initiation in Arabidopsis. Plant Cell **32**: 2543–2565

Abt MR, Zeeman SC (2020) Evolutionary innovations in starch metabolism. Curr Opin Plant Biol **55**: 109–117

Ball S, Guan HP, James M, Myers A, Keeling P, Mouille G, Buleon A, Colonna P, Preiss J (1996) From glycogen to amylopectin: a model for the biogenesis of the plant starch granule. Cell **86**: 349–352

Bao JS (2019) Rice starch. rice: chemistry and technology, 4th edition: 55–108

Boren M, Larsson H, Falk A, Jansson C (2004) The barley starch granule proteome-internalized granule polypeptides of the mature endosperm. Plant Sci **166**: 617–626

Chaen K, Noguchi J, Omori T, Kakuta Y, Kimura M (2012) Crystal structure of the rice branching enzyme I (BEI) in complex with maltopentaose. Biochem Biophys Res Commun **424**: 508–511

Chen HM, Zou Y, Shang YL, Lin HQ, Wang YJ, Cai R, Tang XY, Zhou JM (2008) Firefly luciferase complementation imaging assay for protein-protein interactions in plants. Plant Physiol **146**: 368–376

Chen SB, Tao LZ, Zeng LR, Vega-Sanchez ME, Umemura K, Wang GL (2006) A highly efficient transient protoplast system for analyzing defence gene expression and protein-protein interactions in rice. Mol Plant Pathol **7**: 417–427

Christiansen C, Abou Hachem M, Janecek S, Vikso-Nielsen A, Blennow A, Svensson B (2009) The carbohydrate-binding module family 20 – diversity, structure, and function. FEBS J **276**: 5006–5029

Crofts N, Abe N, Oitome NF, Matsushima R, Hayashi M, Tetlow IJ, Emes MJ, Nakamura Y, Fujita N (2015) Amylopectin biosynthetic enzymes from developing rice seed form enzymatically active protein complexes. J Exp Bot **66**: 4469–4482

David LC, Lee SK, Bruderer E, Abt MR, Fischer-Stettler M, Tschopp MA, Solhaug EM, Sanchez K, Zeeman SC (2022) BETA-AMYLASE9 is a plastidial nonenzymatic regulator of leaf starch degradation. Plant Physiol **188**:191–207

Dian WM, Jiang HW, Chen QS, Liu FY, Wu P (2003) Cloning and characterization of the granule-bound starch synthase II gene in rice: gene expression is regulated by the nitrogen level, sugar and circadian rhythm. Planta **218**: 261–268

Du L, Xu F, Fang J, Gao S, Tang J, Fang S, Wang H, Tong H, Zhang F, Chu J, et al. (2018) Endosperm sugar accumulation caused by mutation of *PHS8*/*ISA1* leads to pre-harvest

sprouting in rice. Plant J **95**: 545–556

Dumez S, Wattebled F, Dauvillee D, Delvalle D, Planchot V, Ball SG, D'Hulst C (2006) Mutants of *Arabidopsis* lacking starch branching enzyme II substitute plastidial starch synthesis by cytoplasmic maltose accumulation. Plant Cell **18**: 2694–2709

Emanuelsson O, Nielsen H, Von Heijne G (1999) ChloroP, a neural network-based method for predicting chloroplast transit peptides and their cleavage sites. Protein Sci **8**: 978–984

Feike D, Seung D, Graf A, Bischof S, Ellick T, Coiro M, Soyk S, Eicke S, Mettler-Altmann T, Lu KJ, et al. (2016) The starch granule-associated protein EARLY STARVATION1 is required for the control of starch degradation in *Arabidopsis thaliana* leaves. Plant Cell **28**: 1472–1489

Fujita N, Kubo A, Suh DS, Wong KS, Jane JL, Ozawa K, Takaiwa F, Inaba Y, Nakamura Y (2003) Antisense inhibition of isoamylase alters the structure of amylopectin and the physicochemical properties of starch in rice endosperm. Plant Cell Physiol **44**: 607–618

Fujita N, Yoshida M, Asakura N, Ohdan T, Miyao A, Hirochika H, Nakamura Y (2006) Function and characterization of starch synthase I using mutants in rice. Plant Physiol **140**: 1070–1084

Grimaud F, Rogniaux H, James MG, Myers AM, Planchot V (2008) Proteome and phosphoproteome analysis of starch granule-associated proteins from normal maize and mutants affected in starch biosynthesis. J Exp Bot **59**: 3395–3406

Hanashiro I, Itoh K, Kuratomi Y, Yamazaki M, Igarashi T, Matsugasako JI, Takeda Y (2008) Granule-bound starch synthase I is responsible for biosynthesis of extra-long unit chains of amylopectin in rice. Plant Cell Physiol **49**: 925–933

Hayashi M, Crofts N, Oitome NF, Fujita N (2018) Analyses of starch biosynthetic protein complexes and starch properties from developing mutant rice seeds with minimal starch synthase activities. BMC Plant Biol **18**: 59

Helle S, Bray F, Verbeke J, Devassine S, Courseaux A, Facon M, Tokarski C, Rolando C, Szydlowski N (2018) Proteome analysis of potato starch reveals the presence of new starch metabolic proteins as well as multiple protease inhibitors. Front. Plant Sci **9:**746

Hiei Y, Ohta S, Komari T, Kumashiro T (1994) Efficient transformation of rice (*Oryza Sativa* L.) mediated by *Agrobacterium* and sequence-analysis of the boundaries of the T-DNA. Plant J **6**: 271–282

Hussain H, Mant A, Seale R, Zeeman S, Hinchliffe E, Edwards A, Hylton C, Bornemann S, Smith AM, Martin C et al. (2003) Three isoforms of isoamylase contribute different catalytic properties for the debranching of potato glucans. Plant Cell **15**: 133–149

James MG, Denyer K, Myers AM (2003) Starch synthesis in the cereal endosperm. Curr Opin Plant Biol **6**: 215–222

Jenkins JPJ, Cameron RE, Donald AM (1993) A universal feature in the structure of starch granules from different botanical sources. Starch-Starke **45**: 417–420

Kang HG, Park S, Matsuoka M, An GH (2005) White-core endosperm *floury endosperm-4* in

rice is generated by knockout mutations in the C_4-type pyruvate orthophosphate dikinase gene (*OsPPDKB*). Plant J **42**: 901–911

Kerk D, Conley TR, Rodriguez FA, Tran HT, Nimick M, Muench DG, Moorhead GB (2006) A chloroplast-localized dual-specificity protein phosphatase in *Arabidopsis* contains a phylogenetically dispersed and ancient carbohydrate-binding domain, which binds the polysaccharide starch. Plant J **46**: 400–413

Kubo A, Fujita N, Harada K, Matsuda T, Satoh H, Nakamura Y (1999) The starch-debranching enzymes isoamylase and pullulanase are both involved in amylopectin biosynthesis in rice endosperm. Plant Physiol **121**: 399–410

Le Corre D, Bras J, Dufresne A (2010) Starch nanoparticles: a review. Biomacromolecules **11**: 1139–1153

Liu C, Pfister B, Osman R, Ritter M, Heutinck A, Sharma M, Eicke S, Fischer-Stettler M, Seung D, Bompard C et al. (2023) LIKE EARLY STARVATION 1 and EARLY STARVATION 1 promote and stabilize amylopectin phase transition in starch biosynthesis. Sci Adv **9**: eadg7448

Liu FS, Romanova N, Lee EA, Ahmed R, Evans M, Gilbert EP, Morell MK, Emes MJ, Tetlow IJ (2012) Glucan affinity of starch synthase IIa determines binding of starch synthase I and starch-branching enzyme IIb to starch granules. Biochem J **448**: 373–387

Liu L, Ma X, Liu S, Zhu C, Jiang L, Wang Y, Shen Y, Ren Y, Dong H, Chen L, et al. (2009) Identification and characterization of a novel *Waxy* allele from a Yunnan rice landrace. Plant Mol Biol **71**: 609–626

Livak KJ, Schmittgen TD (2001) Analysis of relative gene expression data using real-time quantitative PCR and the $2^{-\Delta\Delta CT}$ Method. Methods **25**: 402–408

Lohmeier-Vogel EM, Kerk D, Nimick M, Wrobel S, Vickerman L, Muench DG, Moorhead GB (2008) *Arabidopsis* At5g39790 encodes a chloroplast-localized, carbohydrate-binding, coiled-coil domain-containing putative scaffold protein. BMC Plant Biol **8**: 120

Long WH, Wang YL, Zhu SS, Jing W, Wang YH, Ren YL, Tian YL, Liu SJ, Liu X, Chen LM, et al. (2018) FLOURY SHRUNKEN ENDOSPERM1 connects phospholipid metabolism and amyloplast development in rice. Plant Physiol **177**: 698–712

Matsushima R, Hisano H, Galis I, Miura S, Crofts N, Takenaka Y, Oitome NF, Ishimizu T, Fujita N, Sato K (2023) *FLOURY ENDOSPERM 6* mutations enhance the sugary phenotype caused by the loss of ISOAMYLASE1 in barley. Theor Appl Genet **136**: 94

Matsushima R, Maekawa M, Fujita N, Sakamoto W (2010) A rapid, direct observation method to isolate mutants with defects in starch grain morphology in rice. Plant Cell Physiol **51**: 728–741

Mehrpouyan S, Menon U, Tetlow IJ, Emes MJ (2021) Protein phosphorylation regulates maize endosperm starch synthase IIa activity and protein-protein interactions. Plant J **105**: 1098–1112

Miao J, Guo D, Zhang J, Huang Q, Qin G, Zhang X, Wan J, Gu H, Qu LJ (2013) Targeted

mutagenesis in rice using CRISPR-Cas system. Cell Res **23**: 1233–1236

Myers AM, James MG, Lin QH, Yi G, Stinard PS, Hennen-Bierwagen TA, Becraft PW (2011) Maize *opaque5* encodes monogalactosyldiacylglycerol synthase and specifically affects galactolipids necessary for amyloplast and chloroplast function. Plant Cell **23**: 2331–2347

Nagamatsu S, Wada T, Matsushima R, Fujita N, Miura S, Crofts N, Hosaka Y, Yamaguchi O, Kumamaru T (2022) Mutation in *BEIIb* mitigates the negative effect of the mutation in *ISA1* on grain filling and amyloplast formation in rice. Plant Mol Biol **108**: 497–512

Nakagami T, Yoshihara H, Nakamura T, Utsumi Y, Sawada T, Fujita N, Satoh H, Nakamura Y (2017) Biochemical analysis of new type mutants of japonica rice that accumulate water-soluble-glucans in the endosperm but retain full starch debranching enzyme activities. Starch-Starke **69**: 1600159

Nakamura Y (2002) Towards a better understanding of the metabolic system for amylopectin biosynthesis in plants: rice endosperm as a model tissue. Plant Cell Physiol **43**: 718–725

Nakamura Y, Kubo A, Shimamune T, Matsuda T, Harada K, Satoh H (1997) Correlation between activities of starch debranching enzyme and α-polyglucan structure in endosperms of *sugary-1* mutants of rice. Plant J **12**: 143–153

Nishi A, Nakamura Y, Tanaka N, Satoh H (2001) Biochemical and genetic analysis of the effects of *amylose-extender* mutation in rice endosperm. Plant Physiol **127**: 459–472

Peng C, Wang YH, Liu F, Ren YL, Zhou KN, Lv J, Zheng M, Zhao SL, Zhang L, Wang CM, et al. (2014) *FLOURY ENDOSPERM6* encodes a CBM48 domain-containing protein involved in compound granule formation and starch synthesis in rice endosperm. Plant J **77**: 917–930

Ren Y, Wang Y, Liu F, Zhou K, Ding Y, Zhou F, Wang Y, Liu K, Gan L, Ma W, et al. (2014) *GLUTELIN PRECURSOR ACCUMULATION3* encodes a regulator of post-Golgi vesicular traffic essential for vacuolar protein sorting in rice endosperm. Plant Cell **26**: 410–425

Ren YL, Wang YH, Pan T, Wang YL, Wang YF, Gan L, Wei ZY, Wang F, Wu MM, Jing RN, et al. (2020) *GPA5* encodes a Rab5a effector required for post-Golgi trafficking of rice storage proteins. Plant Cell **32**: 758–777

Seung D, Boudet J, Monroe J, Schreier TB, David LC, Abt M, Lu KJ, Zanella M, Zeemana SC (2017) Homologs of PROTEIN TARGETING TO STARCH control starch granule initiation in *Arabidopsis* leaves. Plant Cell **29**: 1657–1677

Seung D, Schreier TB, Burgy L, Eicke S, Zeeman SC (2018) Two plastidial coiled-coil proteins are essential for normal starch granule initiation in *Arabidopsis*. Plant Cell **30**: 1523–1542

Seung D, Soyk S, Coiro M, Maier BA, Eicke S, Zeeman SC (2015) PROTEIN TARGETING TO STARCH is required for localising GRANULE-BOUND STARCH SYNTHASE to starch granules and for normal amylose synthesis in *Arabidopsis*. PLoS Biol **13**: e1002080

Singh A, Compart J, AL-Rawi SA, Mahto H, Ahmad AM, Fettke J (2022) LIKE EARLY

STARVATION 1 alters the glucan structures at the starch granule surface and thereby influences the action of both starch-synthesizing and starch-degrading enzymes. Plant J **111**: 819–835

Smith AM, Zeeman SC (2020) Starch: a flexible, adaptable carbon store coupled to plant growth. Annu Rev Plant Biol **71**: 217–245

Takahashi K, Kohno H, Kanabayashi T, Okuda M (2019) Glutelin subtype-dependent protein localization in rice grain evidenced by immunodetection analyses. Plant Mol Biol **100**: 231–246

Tamura K, Peterson D, Peterson N, Stecher G, Nei M, Kumar S (2011) MEGA5: molecular evolutionary genetics analysis using maximum likelihood, evolutionary distance, and maximum parsimony methods. Mol Biol Evol **28**: 2731–2739

Thompson DB (2000) On the non-random nature of amylopectin branching. Carbohyd Polym **43**: 223–239

Thompson JD, Higgins DG, Gibson TJ (1994) Clustal W: improving the sensitivity of progressive multiple sequence alignment through sequence weighting, position-specific gap penalties and weight matrix choice. Nucleic Acids Res **22**: 4673–4680

Utsumi Y, Nakamura Y (2006) Structural and enzymatic characterization of the isoamylase1 homo-oligomer and the isoamylase1–isoamylase2 hetero-oligomer from rice endosperm Planta **225**: 75–87

Utsumi Y, Utsumi C, Sawada T, Fujita N, Nakamura Y (2011) Functional diversity of isoamylase oligomers: the ISA1 homo-oligomer is essential for amylopectin biosynthesis in rice endosperm. Plant Physiol **156**: 61–77

Valdez HA, Busi MV, Wayllace NZ, Parisi G, Ugalde RA, Gomez-Casati DF (2008) Role of the N-terminal starch-binding domains in the kinetic properties of starch synthase III from *Arabidopsis thaliana*. Biochemistry. **47**: 3026–3032

Waadt R, Kudla J (2008) In planta visualization of protein interactions using bimolecular fluorescence complementation (BiFC). CSH Protoc **2008**: t4995

Wang L, Zhang WW, Liu SJ, Tian YL, Liu X, Yan HG, Cai Y, Teng X, Dong H, Chen RB, et al. (2021) Rice *FLOURY SHRUNKEN ENDOSPERM 5* encodes a putative plant organelle RNA recognition protein that is required for *cis*-splicing of mitochondrial *nad4* intron 1. Rice **14**: 29

Wang W, Wei XJ, Jiao GA, Chen WQ, Wu YW, Sheng ZH, Hu SK, Xie LH, Wang JY, Tang SQ, et al. (2020) *GBSS-BINDING PROTEIN*, encoding a CBM48 domain-containing protein, affects rice quality and yield. J Integr Plant Biol **62**: 948–966

Wang YH, Ren YL, Liu X, Jiang L, Chen LM, Han XH, Jin MN, Liu SJ, Liu F, Lv J, et al. (2010) OsRab5a regulates endomembrane organization and storage protein trafficking in rice endosperm cells. Plant J **64**: 812–824

Wu MM, Ren YL, Cai MH, Wang YL, Zhu SS, Zhu JP, Hao YY, Teng X, Zhu XP, Jing RN, et al. (2019) Rice *FLOURY ENDOSPERM10* encodes a pentatricopeptide repeat protein

that is essential for the *trans*-splicing of mitochondrial *nad1* intron 1 and endosperm development. New Phytol **223**: 736–750

Wu XB, Liu JX, Li DQ, Liu CM (2016) Rice caryopsis development II: dynamic changes in the endosperm. J Integr Plant Biol **58**: 786–798

You X, Zhang W, Hu J, Jing R, Cai Y, Feng Z, Kong F, Zhang J, Yan H, Chen W, et al. (2019) *FLOURY ENDOSPERM15* encodes a glyoxalase I involved in compound granule formation and starch synthesis in rice endosperm. Plant Cell Rep **38**: 345–359

Zeeman SC, Kossmann J, Smith AM (2010) Starch: its metabolism, evolution, and biotechnological modification in plants. Annu Rev Plant Biol **61**: 209–234

Zhang L, Li N, Zhang J, Zhao L, Qiu J, Wei C (2022) The CBM48 domain-containing protein FLO6 regulates starch synthesis by interacting with SSIVb and GBSS in rice. Plant Mol Biol **108**: 343–361

Zhang L, Ren YL, Lu BY, Yang CY, Feng ZM, Liu Z, Chen J, Ma WW, Wang Y, Yu XW, et al. (2016) *FLOURY ENDOSPERM7* encodes a regulator of starch synthesis and amyloplast development essential for peripheral endosperm development in rice. J Exp Bot **67**: 633–647

Zhao D, Zhang C, Li Q, Liu Q (2022) Genetic control of grain appearance quality in rice. Biotechnol Adv **60**: 108014

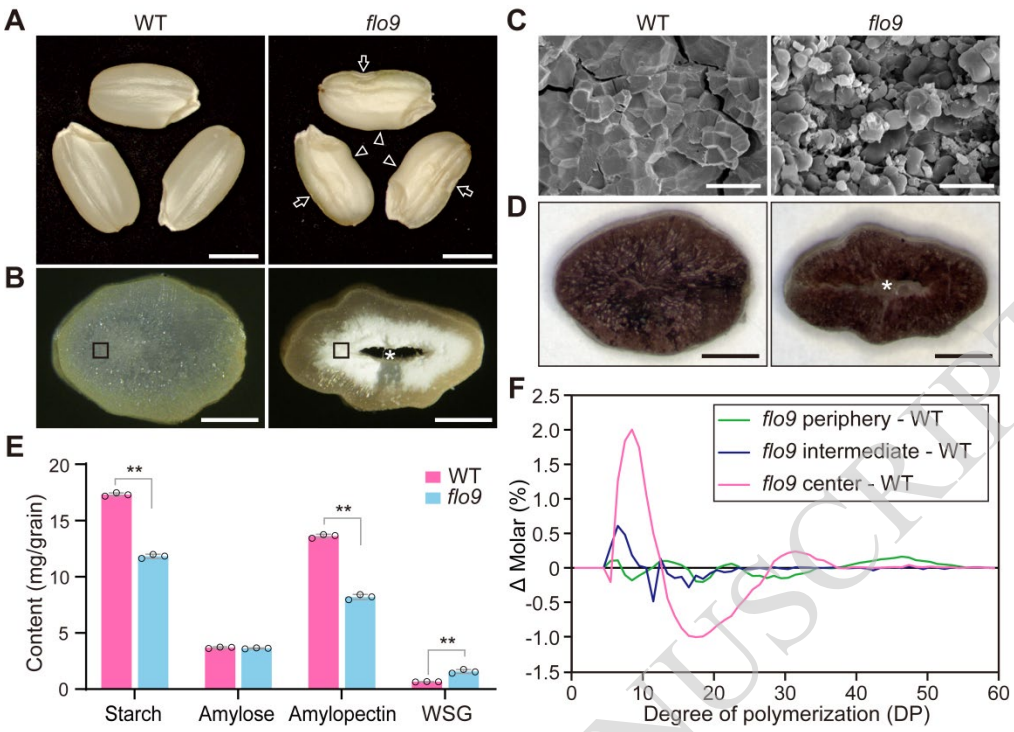

Figure 1. Phenotypic characterization of the *flo9* mutant.

A, Comparison of the representative wild-type (WT) and *flo9* mature grains. Bars = 2 mm. Arrows and arrowheads indicate dimpled indentations and constrictions at the dorsal and ventral sides, respectively.

B, Transverse sections of the representative WT and *flo9* mature grains. Bars = 1 mm. Asterisk indicates the hollow core.

C, Comparison of starch grains (SGs) observed via scanning electron microscope in magnified regions of WT and *flo9* indicated by black squares in (B). Bars = 20 μm.

D, Iodine-stained transverse sections of the representative WT and *flo9* maturing grains at 25 days after flowering (DAF). Bars = 1 mm. Asterisk indicates the hardly-stained core.

E, Determination of total starch, amylose, amylopectin, and water-soluble-glucan (WSG) contents of WT and *flo9* mature grains. Values are means ± SD. $^{**}P < 0.01$ by Student's *t*-test ($n = 3$).

F, Differences in chain length distribution (CLD) patterns of total glucans between WT and *flo9*. Note that rice powder collected from the periphery, intermediate, and center of grains were separately used to determine the glucan CLD.

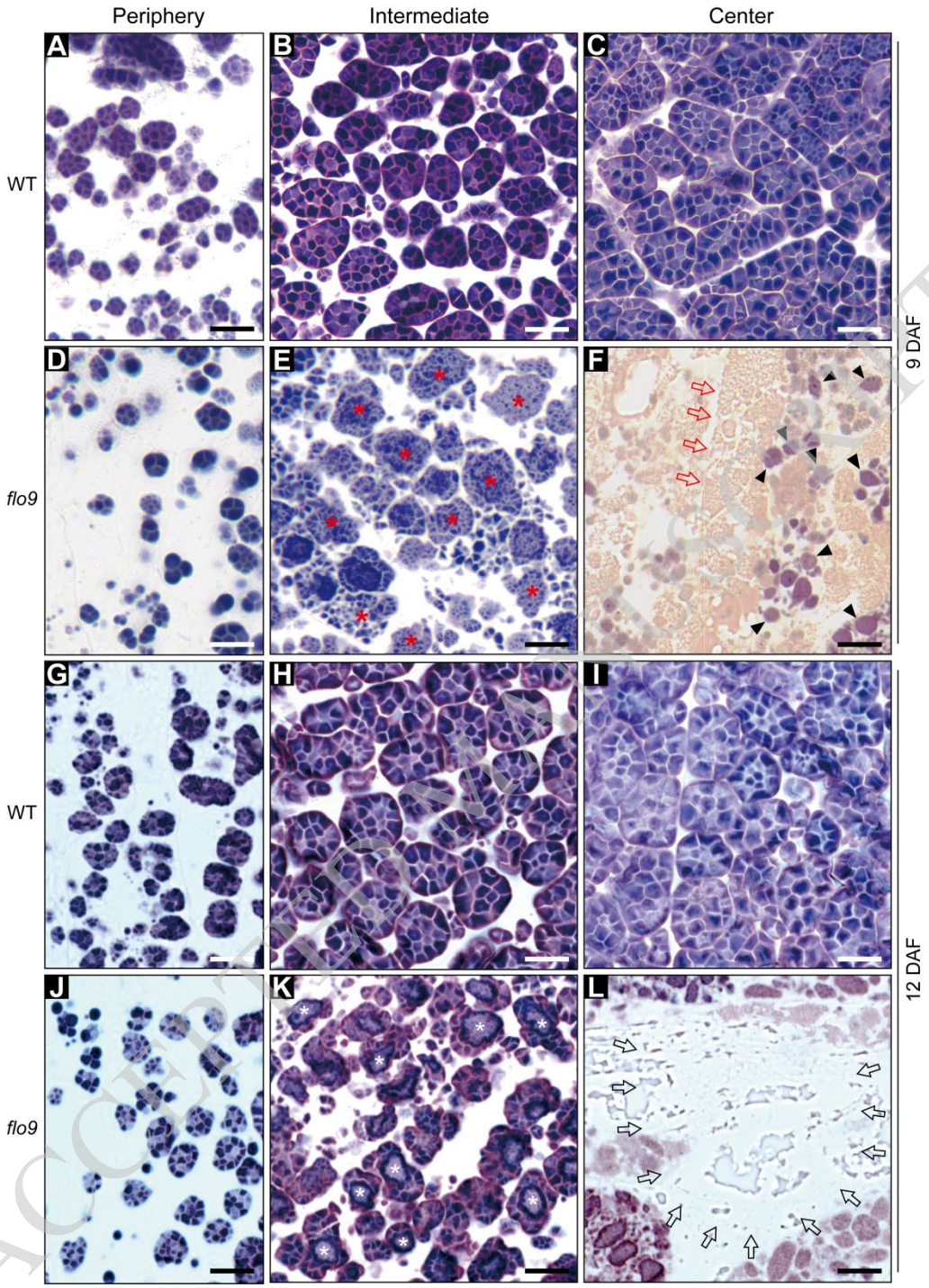

Figure 2. Defects in starch grain (SG) initiation of *flo9* grains.

A–L, Comparison of SGs from iodine-stained semi-thin sections prepared from developing wild-type (WT) and *flo9* endosperm at 9 days after flowering (DAF; A–F) and 12 DAF (G–L). Periphery, intermediate, and center indicate the translucent, floury-white, and hollow regions of *flo9* endosperm, respectively, and the corresponding regions of the WT. Red asterisks in (E) indicate abnormal amyloplasts

containing tiny granules. Black arrowheads in (F) indicate atypical amyloplasts stained weakly with iodine and lacking compound structure. Red arrows in (F) indicate the amorphous SGs filled with pink-stained phytoglycogen-like substances. White asterisks in (K) indicate the amorphous structures with a dark-stained edge in *flo9* amyloplasts. Arrows in (L) outline the contiguous region that is not stained by iodine. Bars = 10 μm.

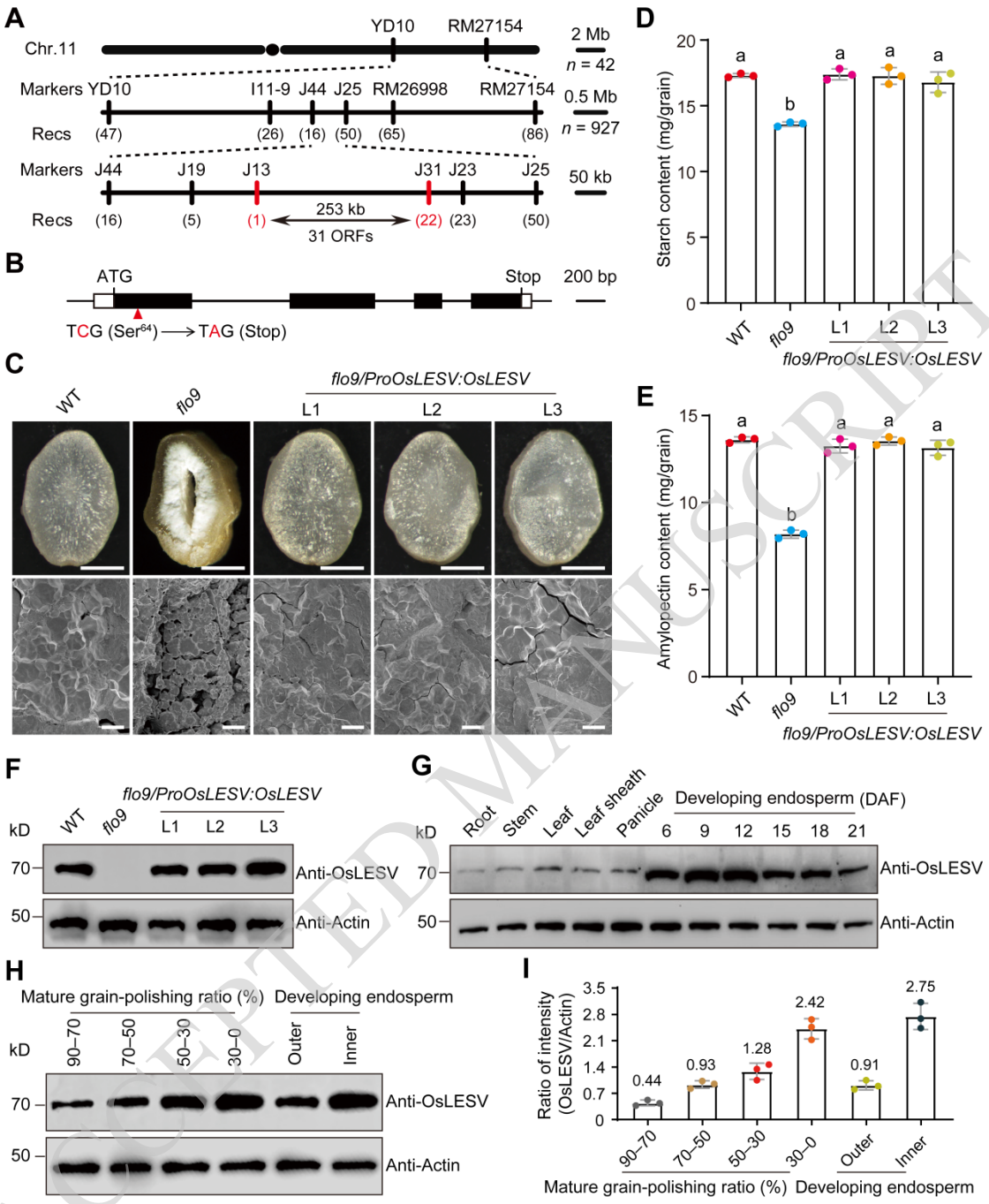

Figure 3. Map-based cloning of the *OsLESV* gene and expression pattern of the OsLESV protein.

A, Fine mapping of the *OsLESV* locus. The *OsLESV* locus was located to a 253-kb region between markers J13 and J31 (red vertical lines). Numbers of recombinants and molecular markers are shown. Chr., chromosome; ORFs, open reading frames; Recs, recombinants.

B, Genomic structure and the mutation site of *OsLESV*. A single nucleotide substitution in the first exon of *OsLESV* led to a premature stop codon in *flo9*. Red arrowhead indicates the mutation site in *flo9*.

C, Expression of the *OsLESV* gene driven by its native promoter restored the grain appearance (the upper panel) and starch grain (SG) morphology (the lower panel). L1 to L3 indicate three independent T_4 generation transgenic lines. Bars in the upper panel = 1 mm; bars in the lower panel = 10 μm. WT, wild type.

D and E, Determination of total starch (D) and amylopectin (E) contents in mature grains of WT, *flo9*, and complemented transgenic lines. Values are means ± SD. $P < 0.05$ by Duncan's multiple range tests ($n = 3$).

F, OsLESV antibodies specifically recognize the endogenous OsLESV protein in total protein extracts of mature grains from WT and complemented transgenic lines but not in *flo9*. Anti-actin antibody was used as a loading control.

G, Protein accumulation profiles of OsLESV in various tissues and different developmental stages of endosperm. DAF, days after flowering. Anti-actin antibody was used as a loading control.

H, Immunoblot analysis of the spatial distribution of OsLESV within endosperm using total protein extracts from different portions of mature grain and developing endosperm by the OsLESV antibodies. Mature grain-polishing ratio refers to the ratio (w/w) of polished rice to the brown rice. Brown rice was sequentially polished to 90%, 70%, 50%, 30% (w/w) of its original weight (approximately 10 g). Rice powder produced at each polishing step was collected as samples with a 90–70%, 70–50%, or 50–30% of grain-polishing ratio. The gradient decrease of grain-polishing ratio indicated that samples were collected from the exterior to the interior of rice endosperm, thus representing the periphery, intermediate, and center of the endosperm, respectively. Anti-actin antibody was used as a loading control. Three independent experiments were performed.

I, Quantification of OsLESV protein in different fractions of (H). The intensity of OsLESV was normalized by the loading control of anti-actin antibody using the Image J software. Values are means ± SD ($n = 3$). The average values were shown on the corresponding columns.

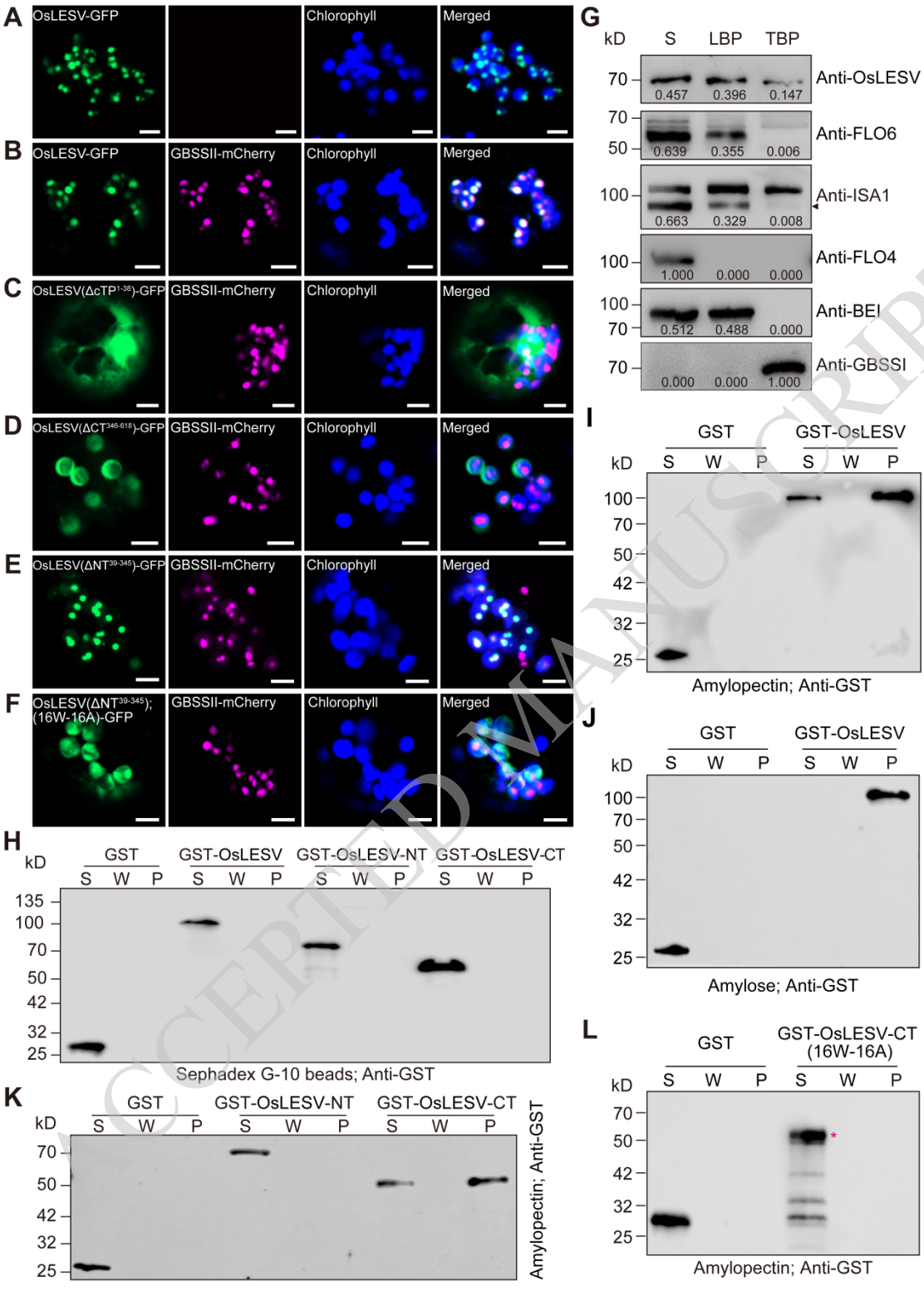

Figure 4. OsLESV binds to starch *in vivo* and *in vitro*.

A, Representative confocal microscopy images showing that OsLESV-GFP is localized to disc-like structures within chloroplasts of rice protoplasts. Blue signals are autofluorescence from chlorophylls in chloroplasts. The rightmost panel represents the merged image of GFP, mCherry, and chlorophyll fluorescence signals. Bars = 5 μm.

B, Representative confocal microscopy images showing that OsLESV-GFP colocalizes with GBSSII-mCherry within chloroplasts of rice protoplasts. Bars = 5 μm.

C–E, Different deletions or mutations of OsLESV-GFP fusion vectors were transiently co-expressed with GBSSII-mCherry in rice protoplasts, respectively. Note that OsLESV($\Delta CT^{346-618}$)-GFP lacking the C-terminal tryptophan (Trp)-rich region displayed a stromal localization pattern, whereas OsLESV(ΔNT^{39-345})-GFP was tightly associated with GBSSII-mCherry within chloroplasts. cTP, chloroplast transit peptide; CT and NT separately indicate the C and N termini of OsLESV. Bars = 5 μm.

F, Representative confocal microscopy images showing that OsLESV(ΔNT^{39-345})-GFP with mutations of 16 evolutionarily conserved Trp to Ala residues abolished its colocalization with starch grains (SGs). NT, N terminus of OsLESV; 16W-16A, the mutation of 16 evolutionarily conserved tryptophan (W) residues to alanine (A) in the tryptophan-rich region of OsLESV. Bars = 5 μm.

G, Association of OsLESV with starch in developing wild-type (WT) endosperm (9 days after flowering). FLO4 (a cytosolic protein), BEI (a granule-associated protein), and GBSSI (a granule-bound protein) were used as marker proteins for different fractions. The volume of each sample subject to SDS-PAGE was 10 μL. LBP, the loosely bound protein; S, the soluble protein; TBP, the tightly bound protein. Arrowhead indicates the target band of ISA1. The relative band intensity of proteins was calculated by image J software. Three independent experiments were performed.

H–J, Binding of recombinant GST-OsLESV protein or its variants to Sephadex G-10 beads (H), amylopectin (I), and amylose (J) *in vitro*. CT and NT separately indicate the C and N termini of OsLESV; GST, glutathione S-transferase; P, the pellet; S, the soluble fraction; W, the final wash.

K, GST-OsLESV-CT recombinant protein but not GST-OsLESV-NT protein specifically bound to amylopectin *in vitro*. CT and NT separately indicate the C and N termini of OsLESV; GST, glutathione S-transferase; P, the pellet; S, the soluble fraction; W, the final wash.

L, Mutations of evolutionarily conserved tryptophan Trp residues in the GST-OsLESV-CT recombinant protein abolished its binding to amylopectin *in vitro*. Equivalent volume (10 μL) of each sample was loaded in (H–L). Asterisk indicates target band of GST-OsLESV-CT(16W-16A) recombinant protein. CT, C terminus of OsLESV. GST, glutathione S-transferase; P, the pellet; S, the soluble fraction; W, the final wash. 16W-16A indicates the mutation of 16 conserved tryptophan (W) residues to alanine (A).

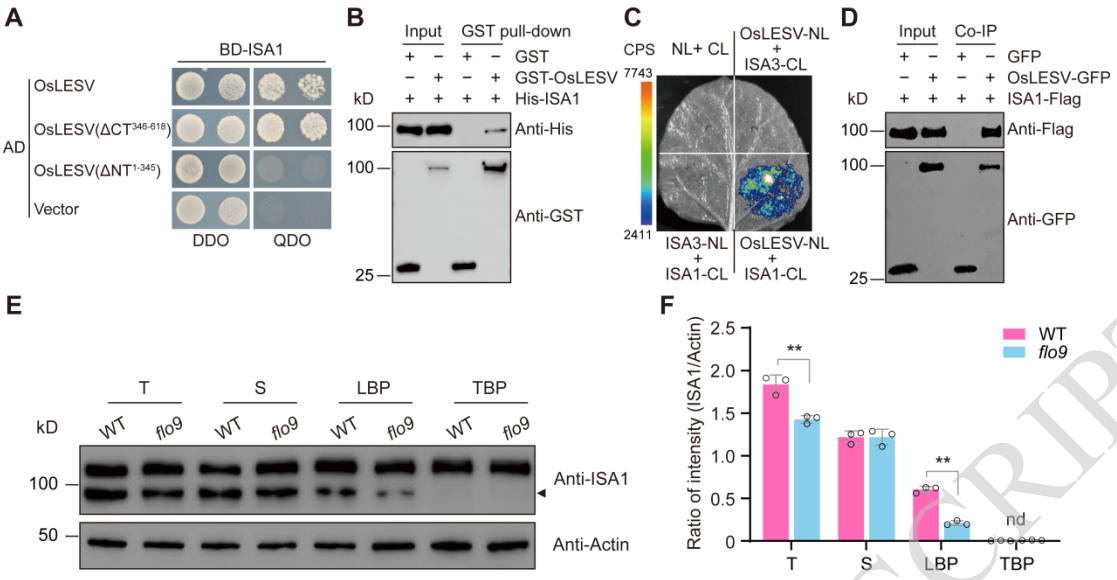

Figure 5. OsLESV physically interacts with ISA1**.**

A, Y2H assay showing that full-length OsLESV and its N terminus interact with ISA1. AD, activation domain; BD, binding domain; CT and NT separately indicate the C and N termini of OsLESV; DDO, control medium (SD/-Trp-Leu); QDO, selective medium (SD/-Trp-Leu-His-Ade). The empty pGADT7 vector was used as a negative control.

B, *In vitro* GST pull-down assay showing that glutathione S-transferase (GST)-tagged OsLESV but not free GST tag could pull down His-tagged ISA1. The symbols "+" or "-" indicates the presence or absence of the corresponding protein.

C, LCI assay showing that OsLESV can specifically interact with ISA1 in *N. benthamiana* leaf epidermal cells. ISA3 was used as a negative control. Colored scale bar indicates the luminescence intensity in counts per second (CPS). NL, N terminus of LUC; CL, C terminus of LUC.

D, CoIP assay verified the interaction between OsLESV and ISA1 in rice protoplasts. ISA1-Flag was transiently coexpressed in rice protoplasts with OsLESV-GFP or free GFP, respectively. ISA1-Flag could be coimmunoprecipitated by OsLESV-GFP but not free GFP using anti-GFP magnetic beads. The symbols "+" or "-" indicates the presence or absence of the corresponding protein.

E, Immunoblot analysis of total ISA1 and its starch association in wild-type (WT) and *flo9* developing endosperm (9 days after flowering). Anti-actin antibody was used as a loading control. The arrowhead indicates the ISA1 band. T, the total protein; LBP, the loosely bound protein; S, the soluble fraction; TBP, the tightly bound protein. Three independent experiments were performed.

F, Quantification of ISA1 protein level in (E). The intensity of ISA1 was normalized by the corresponding intensity of anti-actin antibody using the Image J software. nd, no detection. Values are means ± SD. $^{**}P < 0.01$ by Student's *t*-test ($n = 3$).

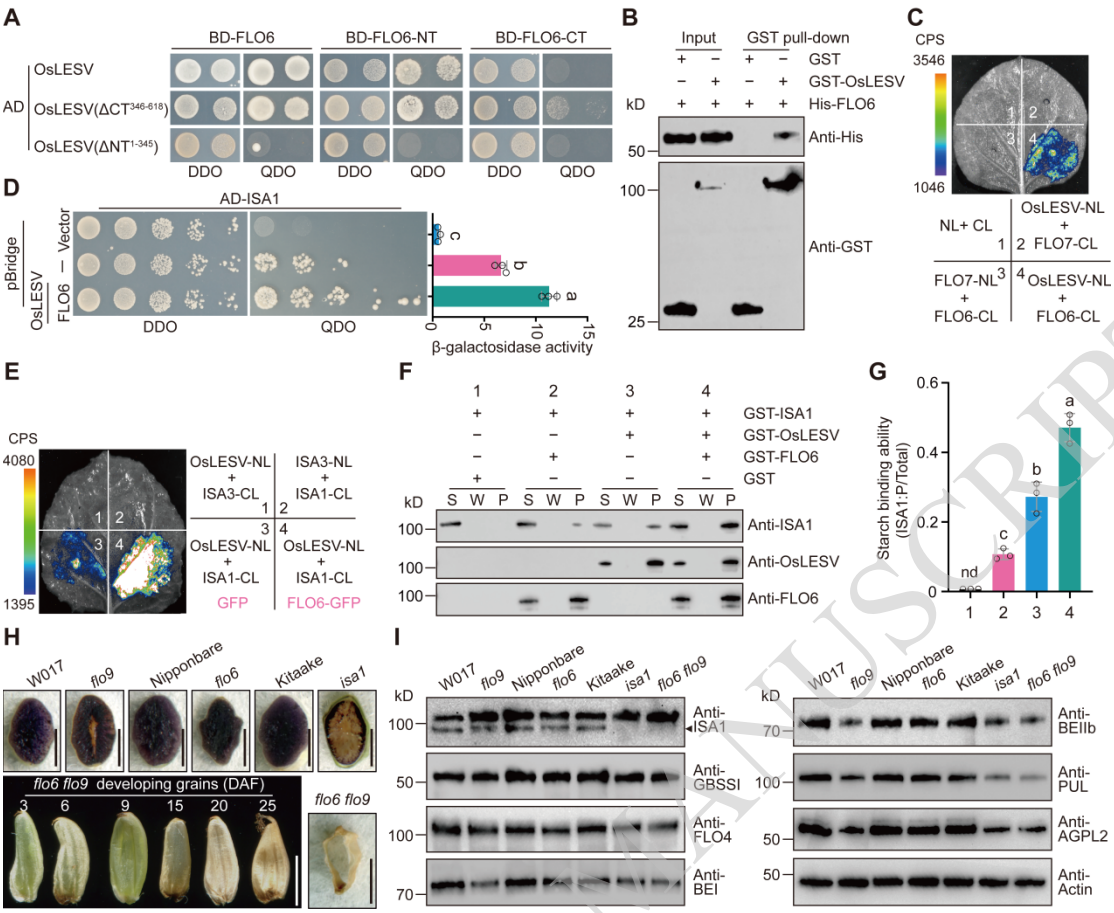

Figure 6. OsLESV physically interacts with FLO6 through their N termini.

A, Y2H analysis showing that OsLESV and FLO6 interact with each other via their N termini. AD, activation domain; BD, binding domain; CT and NT separately indicate the C and N termini of OsLESV or FLO6; DDO, control medium (SD/-Trp-Leu); QDO, selective medium (SD/-Trp-Leu-His-Ade).

B, *In vitro* GST pull-down assay showing that glutathione S-transferase (GST)-tagged OsLESV but not free GST can pull down His-tagged FLO6. The symbols "+" or "-" indicates the presence or absence of the corresponding protein.

C, LCI assay showing that OsLESV can interact with ISA1 in *N. benthamiana* leaf epidermal cells. Chloroplast-localized FLO7 was used as a negative control. Colored scale bar indicates the luminescence intensity in counts per second (CPS). NL, N terminus of LUC; CL, C terminus of LUC.

D, Yeast three-hybrid assay showing that FLO6 can enhance the interaction between OsLESV and ISA1. Note that full-length coding sequence of *OsLESV* was fused to binding domain (MCS I: multiple cloning site I) and driven by constitutive *ADH1* promoter, whereas *FLO6* was inserted into MCS II and driven by a Met-responsive promoter. β-galactosidase activity was measured using CPRG as substrate. Values are

means ± SD. $P < 0.05$ by Duncan's multiple range tests ($n = 3$). AD, activation domain**;** DDO, control medium (SD/-Trp-Leu); QDO, selective medium (SD/-Trp-Leu-His-Ade).

E, LCI assays showing that the FLO6-GFP fusion protein but not free GFP can promote the interaction of OsLESV with ISA1. ISA3 was used as a negative control. Colored scale bar indicates the luminescence intensity in counts per second (CPS). NL, N terminus of LUC; CL, C terminus of LUC.

F, Effects of OsLESV and FLO6 on ISA1 binding to amylopectin *in vitro*. Equal amount of each recombinant protein was combined as indicated and co-incubated with amylopectin for 30 min. Amylopectin was pelleted by centrifugation. Proteins in the supernatant (S), the final wash (W), and the pellet (P) were subject to immunoblot analyses using anti-OsLESV, anti-FLO6, and anti-ISA1 antibodies, respectively. Equivalent volume (10 μL) of each sample was loaded. Three independent experiments were performed. The symbols "+" or "-" indicates the presence or absence of the corresponding protein.

G, Quantification of the ISA1 protein binding to amylopectin in (F). The percentage of starch-binding ISA1 in total ISA1 (S+W+P) was quantified with the Image J software. Values are means ± SD. $P < 0.05$ by Duncan's multiple range tests ($n = 3$). nd, no detection.

H, Phenotypic analyses of the *flo6 flo9* double mutant. Top panel: Iodine-stained transverse-sections of developing grains of W017 (wild type for *flo9*), *flo9*, Nipponbare (wild type for *flo6*), *flo6*, Kitaake (wild type for *isa1*), and *isa1* at 25 DAF. Bottom panel: The left shows the developing *flo6 flo9* caryopsis from 3 to 25 days after flowering (DAF) (numbers above denote the DAF). Note that the core region of *flo9* as well as most of the *isa1* endosperm were not stained by iodine. The right shows a transverse-section of the *flo6 flo9* grain at 25 DAF. Bars = 2 mm.

I, Immunoblot analysis of starch synthesis-related enzymes protein abundance in total protein extracts of developing endosperm of the *flo9*, *flo6*, and *isa1* single mutant, and their corresponding wild type, as well as the double mutant *flo6 flo9* at 25 DAF. Anti-actin antibody was used as a loading control. The arrowhead indicates the band of ISA1.

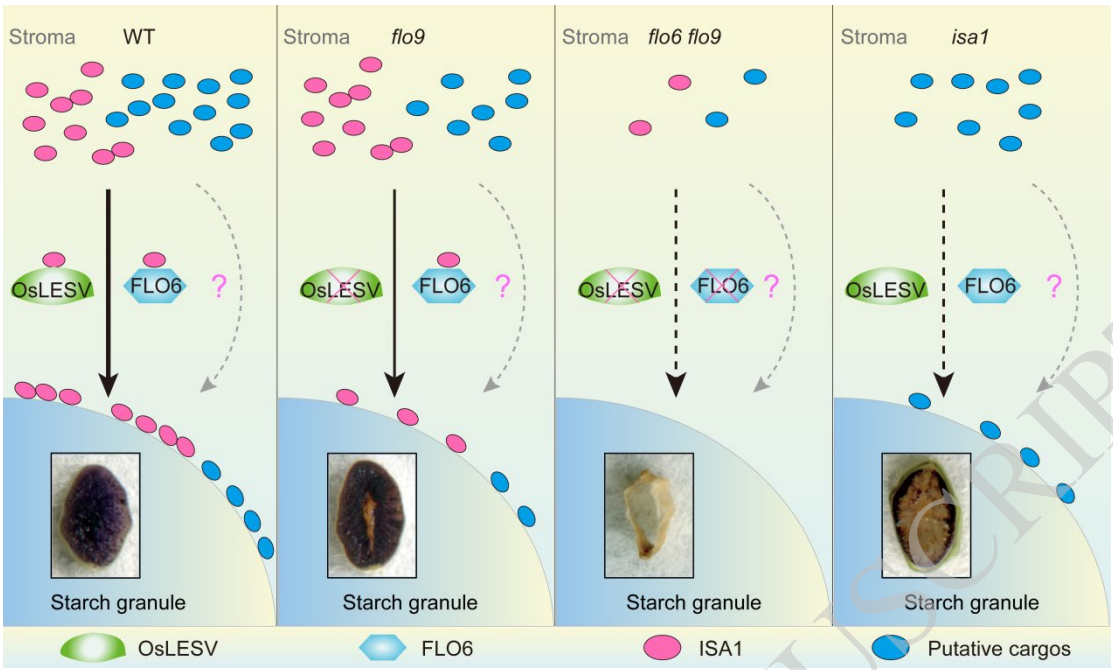

Figure 7. Working model for the OsLESV-FLO6 molecular module in facilitating ISA1 binding to starch granules in rice endosperm.

In the wild-type (WT) endosperm, OsLESV and FLO6 form a functional protein complex to recruit ISA1 from the stroma to starch granules, where ISA1 is responsible for the removal of misplaced branches in amylopectin. Loss of *OsLESV* function considerably compromises the distribution of ISA1 onto starch granules, whereas loss-of-function mutations of both *OsLESV* and *FLO6* substantially decreased the protein abundance of ISA1, and dramatically disrupted starch biosynthesis and endosperm development. Loss of *ISA1* function accumulates large amounts of phytoglycogen instead of starch, and thus disrupts the formation of higher-order amylopectin structure and amylopectin crystallizing. The thick solid arrow indicates an effective targeting of ISA1 to starch granules, while the thin solid arrow and dashed black arrows indicate weak and disturbed binding of ISA1 to starch granules, respectively. In addition, the dotted grey arrow indicates a possible functional role of OsLESV and FLO6 in the delivery of other unknown cargos onto starch granules during starch biosynthesis. Insets inside of starch granule model denote the I_2-KI staining of transverse sections of corresponding grains.

Parsed Citations

Abt MR, Pfister B, Sharma M, Eicke S, Burgy L, Neale I, Seung D, Zeeman SC (2020) STARCH SYNTHASE5, a noncanonical starch synthase-like protein, promotes starch granule initiation in Arabidopsis. Plant Cell 32: 2543–2565
Google Scholar: Author Only Title Only Author and Title

Abt MR, Zeeman SC (2020) Evolutionary innovations in starch metabolism. Curr Opin Plant Biol 55: 109–117
Google Scholar: Author Only Title Only Author and Title

Ball S, Guan HP, James M, Myers A, Keeling P, Mouille G, Buleon A, Colonna P, Preiss J (1996) From glycogen to amylopectin: a model for the biogenesis of the plant starch granule. Cell 86: 349–352
Google Scholar: Author Only Title Only Author and Title

Bao JS (2019) Rice starch. rice: chemistry and technology, 4th edition: 55–108
Google Scholar: Author Only Title Only Author and Title

Boren M, Larsson H, Falk A, Jansson C (2004) The barley starch granule proteome-internalized granule polypeptides of the mature endosperm. Plant Sci 166: 617–626
Google Scholar: Author Only Title Only Author and Title

Chaen K, Noguchi J, Omori T, Kakuta Y, Kimura M (2012) Crystal structure of the rice branching enzyme I (BEI) in complex with maltopentaose. Biochem Biophys Res Commun 424: 508–511
Google Scholar: Author Only Title Only Author and Title

Chen HM, Zou Y, Shang YL, Lin HQ, Wang YJ, Cai R, Tang XY, Zhou JM (2008) Firefly luciferase complementation imaging assay for protein-protein interactions in plants. Plant Physiol 146: 368–376
Google Scholar: Author Only Title Only Author and Title

Chen SB, Tao LZ, Zeng LR, Vega-Sanchez ME, Umemura K, Wang GL (2006) A highly efficient transient protoplast system for analyzing defence gene expression and protein-protein interactions in rice. Mol Plant Pathol 7: 417–427
Google Scholar: Author Only Title Only Author and Title

Christiansen C, Abou Hachem M, Janecek S, Vikso-Nielsen A, Blennow A, Svensson B (2009) The carbohydrate-binding module family 20 – diversity, structure, and function. FEBS J 276: 5006–5029
Google Scholar: Author Only Title Only Author and Title

Crofts N, Abe N, Oitome NF, Matsushima R, Hayashi M, Tetlow IJ, Emes MJ, Nakamura Y, Fujita N (2015) Amylopectin biosynthetic enzymes from developing rice seed form enzymatically active protein complexes. J Exp Bot 66: 4469–4482
Google Scholar: Author Only Title Only Author and Title

David LC, Lee SK, Bruderer E, Abt MR, Fischer-Stettler M, Tschopp MA, Solhaug EM, Sanchez K, Zeeman SC (2022) BETA-AMYLASE9 is a plastidial nonenzymatic regulator of leaf starch degradation. Plant Physiol 188:191–207
Google Scholar: Author Only Title Only Author and Title

Dian WM, Jiang HW, Chen QS, Liu FY, Wu P (2003) Cloning and characterization of the granule-bound starch synthase II gene in rice: gene expression is regulated by the nitrogen level, sugar and circadian rhythm. Planta 218: 261–268
Google Scholar: Author Only Title Only Author and Title

Du L, Xu F, Fang J, Gao S, Tang J, Fang S, Wang H, Tong H, Zhang F, Chu J, et al. (2018) Endosperm sugar accumulation caused by mutation of PHS8/ISA1 leads to pre-harvest sprouting in rice. Plant J 95: 545–556
Google Scholar: Author Only Title Only Author and Title

Dumez S, Wattebled F, Dauvillee D, Delvalle D, Planchot V, Ball SG, D'Hulst C (2006) Mutants of Arabidopsis lacking starch branching enzyme II substitute plastidial starch synthesis by cytoplasmic maltose accumulation. Plant Cell 18: 2694–2709
Google Scholar: Author Only Title Only Author and Title

Emanuelsson O, Nielsen H, Von Heijne G (1999) ChloroP, a neural network-based method for predicting chloroplast transit peptides and their cleavage sites. Protein Sci 8: 978–984
Google Scholar: Author Only Title Only Author and Title

Feike D, Seung D, Graf A, Bischof S, Ellick T, Coiro M, Soyk S, Eicke S, Mettler-Altmann T, Lu KJ, et al. (2016) The starch granule-associated protein EARLY STARVATION1 is required for the control of starch degradation in Arabidopsis thaliana leaves. Plant Cell 28: 1472–1489
Google Scholar: Author Only Title Only Author and Title

Fujita N, Kubo A, Suh DS, Wong KS, Jane JL, Ozawa K, Takaiwa F, Inaba Y, Nakamura Y (2003) Antisense inhibition of isoamylase alters the structure of amylopectin and the physicochemical properties of starch in rice endosperm. Plant Cell Physiol 44: 607–618
Google Scholar: Author Only Title Only Author and Title

Fujita N, Yoshida M, Asakura N, Ohdan T, Miyao A, Hirochika H, Nakamura Y (2006) Function and characterization of starch synthase I using mutants in rice. Plant Physiol 140: 1070–1084
Google Scholar: Author Only Title Only Author and Title

Grimaud F, Rogniaux H, James MG, Myers AM, Planchot V (2008) Proteome and phosphoproteome analysis of starch granule-associated proteins from normal maize and mutants affected in starch biosynthesis. J Exp Bot 59: 3395–3406
Google Scholar: Author Only Title Only Author and Title

Hanashiro I, Itoh K, Kuratomi Y, Yamazaki M, Igarashi T, Matsugasako JI, Takeda Y (2008) Granule-bound starch synthase I is responsible for biosynthesis of extra-long unit chains of amylopectin in rice. Plant Cell Physiol 49: 925–933
Google Scholar: Author Only Title Only Author and Title

Hayashi M, Crofts N, Oitome NF, Fujita N (2018) Analyses of starch biosynthetic protein complexes and starch properties from developing mutant rice seeds with minimal starch synthase activities. BMC Plant Biol 18: 59
Google Scholar: Author Only Title Only Author and Title

Helle S, Bray F, Verbeke J, Devassine S, Courseaux A, Facon M, Tokarski C, Rolando C, Szydlowski N (2018) Proteome analysis of potato starch reveals the presence of new starch metabolic proteins as well as multiple protease inhibitors. Front. Plant Sci 9:746
Google Scholar: Author Only Title Only Author and Title

Hiei Y, Ohta S, Komari T, Kumashiro T (1994) Efficient transformation of rice (Oryza Sativa L.) mediated by Agrobacterium and sequence-analysis of the boundaries of the T-DNA. Plant J 6: 271–282
Google Scholar: Author Only Title Only Author and Title

Hussain H, Mant A, Seale R, Zeeman S, Hinchliffe E, Edwards A, Hylton C, Bornemann S, Smith AM, Martin C et al. (2003) Three isoforms of isoamylase contribute different catalytic properties for the debranching of potato glucans. Plant Cell 15: 133–149
Google Scholar: Author Only Title Only Author and Title

James MG, Denyer K, Myers AM (2003) Starch synthesis in the cereal endosperm. Curr Opin Plant Biol 6: 215–222
Google Scholar: Author Only Title Only Author and Title

Jenkins JPJ, Cameron RE, Donald AM (1993) A universal feature in the structure of starch granules from different botanical sources. Starch-Starke 45: 417–420
Google Scholar: Author Only Title Only Author and Title

Kang HG, Park S, Matsuoka M, An GH (2005) White-core endosperm floury endosperm-4 in rice is generated by knockout mutations in the C4-type pyruvate orthophosphate dikinase gene (OsPPDKB). Plant J 42: 901–911
Google Scholar: Author Only Title Only Author and Title

Kerk D, Conley TR, Rodriguez FA, Tran HT, Nimick M, Muench DG, Moorhead GB (2006) A chloroplast-localized dual-specificity protein phosphatase in Arabidopsis contains a phylogenetically dispersed and ancient carbohydrate-binding domain, which binds the polysaccharide starch. Plant J 46: 400–413
Google Scholar: Author Only Title Only Author and Title

Kubo A, Fujita N, Harada K, Matsuda T, Satoh H, Nakamura Y (1999) The starch-debranching enzymes isoamylase and pullulanase are both involved in amylopectin biosynthesis in rice endosperm. Plant Physiol 121: 399–410
Google Scholar: Author Only Title Only Author and Title

Le Corre D, Bras J, Dufresne A (2010) Starch nanoparticles: a review. Biomacromolecules 11: 1139–1153
Google Scholar: Author Only Title Only Author and Title

Liu C, Pfister B, Osman R, Ritter M, Heutinck A, Sharma M, Eicke S, Fischer-Stettler M, Seung D, Bompard C et al. (2023) LIKE EARLY STARVATION 1 and EARLY STARVATION 1 promote and stabilize amylopectin phase transition in starch biosynthesis. Sci Adv 9: eadg7448
Google Scholar: Author Only Title Only Author and Title

Liu FS, Romanova N, Lee EA, Ahmed R, Evans M, Gilbert EP, Morell MK, Emes MJ, Tetlow IJ (2012) Glucan affinity of starch synthase IIa determines binding of starch synthase I and starch-branching enzyme IIb to starch granules. Biochem J 448: 373–387
Google Scholar: Author Only Title Only Author and Title

Liu L, Ma X, Liu S, Zhu C, Jiang L, Wang Y, Shen Y, Ren Y, Dong H, Chen L, et al. (2009) Identification and characterization of a novel Waxy allele from a Yunnan rice landrace. Plant Mol Biol 71: 609–626
Google Scholar: Author Only Title Only Author and Title

Livak KJ, Schmittgen TD (2001) Analysis of relative gene expression data using real-time quantitative PCR and the 2-ΔΔCT Method. Methods 25: 402–408
Google Scholar: Author Only Title Only Author and Title

Lohmeier-Vogel EM, Kerk D, Nimick M, Wrobel S, Vickerman L, Muench DG, Moorhead GB (2008) Arabidopsis At5g39790 encodes

a chloroplast-localized, carbohydrate-binding, coiled-coil domain-containing putative scaffold protein. BMC Plant Biol 8: 120
Google Scholar: Author Only Title Only Author and Title

Long WH, Wang YL, Zhu SS, Jing W, Wang YH, Ren YL, Tian YL, Liu SJ, Liu X, Chen LM, et al. (2018) FLOURY SHRUNKEN ENDOSPERM1 connects phospholipid metabolism and amyloplast development in rice. Plant Physiol 177: 698–712
Google Scholar: Author Only Title Only Author and Title

Matsushima R, Hisano H, Galis I, Miura S, Crofts N, Takenaka Y, Oitome NF, Ishimizu T, Fujita N, Sato K (2023) FLOURY ENDOSPERM 6 mutations enhance the sugary phenotype caused by the loss of ISOAMYLASE1 in barley. Theor Appl Genet 136: 94
Google Scholar: Author Only Title Only Author and Title

Matsushima R, Maekawa M, Fujita N, Sakamoto W (2010) A rapid, direct observation method to isolate mutants with defects in starch grain morphology in rice. Plant Cell Physiol 51: 728–741
Google Scholar: Author Only Title Only Author and Title

Mehrpouyan S, Menon U, Tetlow IJ, Emes MJ (2021) Protein phosphorylation regulates maize endosperm starch synthase IIa activity and protein-protein interactions. Plant J 105: 1098–1112
Google Scholar: Author Only Title Only Author and Title

Miao J, Guo D, Zhang J, Huang Q, Qin G, Zhang X, Wan J, Gu H, Qu LJ (2013) Targeted mutagenesis in rice using CRISPR-Cas system. Cell Res 23: 1233–1236
Google Scholar: Author Only Title Only Author and Title

Myers AM, James MG, Lin QH, Yi G, Stinard PS, Hennen-Bierwagen TA, Becraft PW (2011) Maize opaque5 encodes monogalactosyldiacylglycerol synthase and specifically affects galactolipids necessary for amyloplast and chloroplast function. Plant Cell 23: 2331–2347
Google Scholar: Author Only Title Only Author and Title

Nagamatsu S, Wada T, Matsushima R, Fujita N, Miura S, Crofts N, Hosaka Y, Yamaguchi O, Kumamaru T (2022) Mutation in BEIIb mitigates the negative effect of the mutation in ISA1 on grain filling and amyloplast formation in rice. Plant Mol Biol 108: 497–512
Google Scholar: Author Only Title Only Author and Title

Nakagami T, Yoshihara H, Nakamura T, Utsumi Y, Sawada T, Fujita N, Satoh H, Nakamura Y (2017) Biochemical analysis of new type mutants of japonica rice that accumulate water-soluble-glucans in the endosperm but retain full starch debranching enzyme activities. Starch-Starke 69: 1600159
Google Scholar: Author Only Title Only Author and Title

Nakamura Y (2002) Towards a better understanding of the metabolic system for amylopectin biosynthesis in plants: rice endosperm as a model tissue. Plant Cell Physiol 43: 718–725
Google Scholar: Author Only Title Only Author and Title

Nakamura Y, Kubo A, Shimamune T, Matsuda T, Harada K, Satoh H (1997) Correlation between activities of starch debranching enzyme and α-polyglucan structure in endosperms of sugary-1 mutants of rice. Plant J 12: 143–153
Google Scholar: Author Only Title Only Author and Title

Nishi A, Nakamura Y, Tanaka N, Satoh H (2001) Biochemical and genetic analysis of the effects of amylose-extender mutation in rice endosperm. Plant Physiol 127: 459–472
Google Scholar: Author Only Title Only Author and Title

Peng C, Wang YH, Liu F, Ren YL, Zhou KN, Lv J, Zheng M, Zhao SL, Zhang L, Wang CM, et al. (2014) FLOURY ENDOSPERM6 encodes a CBM48 domain-containing protein involved in compound granule formation and starch synthesis in rice endosperm. Plant J 77: 917–930
Google Scholar: Author Only Title Only Author and Title

Ren Y, Wang Y, Liu F, Zhou K, Ding Y, Zhou F, Wang Y, Liu K, Gan L, Ma W, et al. (2014) GLUTELIN PRECURSOR ACCUMULATION3 encodes a regulator of post-Golgi vesicular traffic essential for vacuolar protein sorting in rice endosperm. Plant Cell 26: 410–425
Google Scholar: Author Only Title Only Author and Title

Ren YL, Wang YH, Pan T, Wang YL, Wang YF, Gan L, Wei ZY, Wang F, Wu MM, Jing RN, et al. (2020) GPA5 encodes a Rab5a effector required for post-Golgi trafficking of rice storage proteins. Plant Cell 32: 758–777
Google Scholar: Author Only Title Only Author and Title

Seung D, Boudet J, Monroe J, Schreier TB, David LC, Abt M, Lu KJ, Zanella M, Zeeman SC (2017) Homologs of PROTEIN TARGETING TO STARCH control starch granule initiation in Arabidopsis leaves. Plant Cell 29: 1657–1677
Google Scholar: Author Only Title Only Author and Title

Seung D, Schreier TB, Burgy L, Eicke S, Zeeman SC (2018) Two plastidial coiled-coil proteins are essential for normal starch granule initiation in Arabidopsis. Plant Cell 30: 1523–1542

Google Scholar: Author Only Title Only Author and Title

Seung D, Soyk S, Coiro M, Maier BA, Eicke S, Zeeman SC (2015) PROTEIN TARGETING TO STARCH is required for localising GRANULE-BOUND STARCH SYNTHASE to starch granules and for normal amylose synthesis in Arabidopsis. PLoS Biol 13: e1002080
Google Scholar: Author Only Title Only Author and Title

Singh A, Compart J, AL-Rawi SA, Mahto H, Ahmad AM, Fettke J (2022) LIKE EARLY STARVATION 1 alters the glucan structures at the starch granule surface and thereby influences the action of both starch-synthesizing and starch-degrading enzymes. Plant J 111: 819–835
Google Scholar: Author Only Title Only Author and Title

Smith AM, Zeeman SC (2020) Starch: a flexible, adaptable carbon store coupled to plant growth. Annu Rev Plant Biol 71: 217–245
Google Scholar: Author Only Title Only Author and Title

Takahashi K, Kohno H, Kanabayashi T, Okuda M (2019) Glutelin subtype-dependent protein localization in rice grain evidenced by immunodetection analyses. Plant Mol Biol 100: 231–246
Google Scholar: Author Only Title Only Author and Title

Tamura K, Peterson D, Peterson N, Stecher G, Nei M, Kumar S (2011) MEGA5: molecular evolutionary genetics analysis using maximum likelihood, evolutionary distance, and maximum parsimony methods. Mol Biol Evol 28: 2731–2739
Google Scholar: Author Only Title Only Author and Title

Thompson DB (2000) On the non-random nature of amylopectin branching. Carbohyd Polym 43: 223–239
Google Scholar: Author Only Title Only Author and Title

Thompson JD, Higgins DG, Gibson TJ (1994) Clustal W: improving the sensitivity of progressive multiple sequence alignment through sequence weighting, position-specific gap penalties and weight matrix choice. Nucleic Acids Res 22: 4673–4680
Google Scholar: Author Only Title Only Author and Title

Utsumi Y, Nakamura Y (2006) Structural and enzymatic characterization of the isoamylase1 homo-oligomer and the isoamylase1–isoamylase2 hetero-oligomer from rice endosperm Planta 225: 75–87

Utsumi Y, Utsumi C, Sawada T, Fujita N, Nakamura Y (2011) Functional diversity of isoamylase oligomers: the ISA1 homo-oligomer is essential for amylopectin biosynthesis in rice endosperm. Plant Physiol 156: 61–77
Google Scholar: Author Only Title Only Author and Title

Valdez HA, Busi MV, Wayllace NZ, Parisi G, Ugalde RA, Gomez-Casati DF (2008) Role of the N-terminal starch-binding domains in the kinetic properties of starch synthase III from Arabidopsis thaliana. Biochemistry. 47: 3026–3032
Google Scholar: Author Only Title Only Author and Title

Waadt R, Kudla J (2008) In planta visualization of protein interactions using bimolecular fluorescence complementation (BiFC). CSH Protoc 2008: t4995
Google Scholar: Author Only Title Only Author and Title

Wang L, Zhang WW, Liu SJ, Tian YL, Liu X, Yan HG, Cai Y, Teng X, Dong H, Chen RB, et al. (2021) Rice FLOURY SHRUNKEN ENDOSPERM 5 encodes a putative plant organelle RNA recognition protein that is required for cis-splicing of mitochondrial nad4 intron 1. Rice 14: 29
Google Scholar: Author Only Title Only Author and Title

Wang W, Wei XJ, Jiao GA, Chen WQ, Wu YW, Sheng ZH, Hu SK, Xie LH, Wang JY, Tang SQ, et al. (2020) GBSS-BINDING PROTEIN, encoding a CBM48 domain-containing protein, affects rice quality and yield. J Integr Plant Biol 62: 948–966
Google Scholar: Author Only Title Only Author and Title

Wang YH, Ren YL, Liu X, Jiang L, Chen LM, Han XH, Jin MN, Liu SJ, Liu F, Lv J, et al. (2010) OsRab5a regulates endomembrane organization and storage protein trafficking in rice endosperm cells. Plant J 64: 812–824
Google Scholar: Author Only Title Only Author and Title

Wu MM, Ren YL, Cai MH, Wang YL, Zhu SS, Zhu JP, Hao YY, Teng X, Zhu XP, Jing RN, et al. (2019) Rice FLOURY ENDOSPERM10 encodes a pentatricopeptide repeat protein that is essential for the trans-splicing of mitochondrial nad1 intron 1 and endosperm development. New Phytol 223: 736–750
Google Scholar: Author Only Title Only Author and Title

Wu XB, Liu JX, Li DQ, Liu CM (2016) Rice caryopsis development II: dynamic changes in the endosperm. J Integr Plant Biol 58: 786–798
Google Scholar: Author Only Title Only Author and Title

You X, Zhang W, Hu J, Jing R, Cai Y, Feng Z, Kong F, Zhang J, Yan H, Chen W, et al. (2019) FLOURY ENDOSPERM15 encodes a glyoxalase I involved in compound granule formation and starch synthesis in rice endosperm. Plant Cell Rep 38: 345–359
Google Scholar: Author Only Title Only Author and Title

Zeeman SC, Kossmann J, Smith AM (2010) Starch: its metabolism, evolution, and biotechnological modification in plants. Annu Rev Plant Biol 61: 209–234
Google Scholar: Author Only Title Only Author and Title

Zhang L, Li N, Zhang J, Zhao L, Qiu J, Wei C (2022) The CBM48 domain-containing protein FLO6 regulates starch synthesis by interacting with SSIVb and GBSS in rice. Plant Mol Biol 108: 343–361
Google Scholar: Author Only Title Only Author and Title

Zhang L, Ren YL, Lu BY, Yang CY, Feng ZM, Liu Z, Chen J, Ma WW, Wang Y, Yu XW, et al. (2016) FLOURY ENDOSPERM7 encodes a regulator of starch synthesis and amyloplast development essential for peripheral endosperm development in rice. J Exp Bot 67: 633–647
Google Scholar: Author Only Title Only Author and Title

Zhao D, Zhang C, Li Q, Liu Q (2022) Genetic control of grain appearance quality in rice. Biotechnol Adv 60: 108014
Google Scholar: Author Only Title Only Author and Title